JEM Journal of Experimental Medicine

ARTICLE

Engrailed 1 coordinates cytoskeletal reorganization to induce myofibroblast differentiation

Andrea-Hermina Györfi[1,2*], Alexandru-Emil Matei[1,2*], Maximilian Fuchs[3], Chunguang Liang[3], Aleix Rius Rigau[1,2], Xuezhi Hong[1,2], Honglin Zhu[1,2,4], Markus Luber[1,2], Christina Bergmann[1,2], Clara Dees[1,2], Ingo Ludolph[5], Raymund E. Horch[5], Oliver Distler[6], Jiucun Wang[7,8,9], Bertram Bengsch[10,11], Georg Schett[1,2], Meik Kunz[3], and Jörg H.W. Distler[1,2]

Transforming growth factor-β (TGFβ) is a key mediator of fibroblast activation in fibrotic diseases, including systemic sclerosis. Here we show that Engrailed 1 (EN1) is reexpressed in multiple fibroblast subpopulations in the skin of SSc patients. We characterize EN1 as a molecular amplifier of TGFβ signaling in myofibroblast differentiation: TGFβ induces EN1 expression in a SMAD3-dependent manner, and in turn, EN1 mediates the profibrotic effects of TGFβ. RNA sequencing demonstrates that EN1 induces a profibrotic gene expression profile functionally related to cytoskeleton organization and ROCK activation. EN1 regulates gene expression by modulating the activity of SP1 and other SP transcription factors, as confirmed by ChIP-seq experiments for EN1 and SP1. Functional experiments confirm the coordinating role of EN1 on ROCK activity and the reorganization of cytoskeleton during myofibroblast differentiation, in both standard fibroblast culture systems and in vitro skin models. Consistently, mice with fibroblast-specific knockout of *En1* demonstrate impaired fibroblast-to-myofibroblast transition and are partially protected from experimental skin fibrosis.

Introduction

Fibrotic diseases are a major cause of morbidity and mortality, accounting for ≤40% of the deaths in Western societies (Wynn, 2008). Systemic sclerosis (SSc) is the prototypical systemic fibrotic disease, characterized by excessive deposition of collagen in skin and multiple other organs, leading to their dysfunction (Gabrielli et al., 2009). The major effector cells in fibrosis are activated fibroblasts, so-called myofibroblasts, which express contractile proteins such as α-smooth muscle actin (αSMA) and produce excess collagen (Hinz et al., 2012; Wynn and Ramalingam, 2012). Resting fibroblasts are initially activated by cytokines released from infiltrating leukocytes, both in physiological responses such as wound healing and in fibrosis (Distler et al., 2019). Of these cytokines, TGFβ plays a key role, driving persistent fibroblast activation not only during disease initiation, but also at later stages of fibrosis, when the inflammation has subsided and fibroblasts remain endogenously activated (Distler et al., 2019). TGFβ activates fibroblasts via a complex network of multiple intracellular cascades (Lafyatis, 2014). These TGFβ-regulated intracellular pathways are main targets of emerging antifibrotic therapies (Györfi et al., 2018). Thus, discovery and characterization of novel mediators of the profibrotic effects of TGFβ can provide new therapeutic opportunities in SSc (Distler et al., 2017).

Engrailed 1 (EN1) is a homeodomain-containing transcription factor with essential, widespread roles in embryonic development of different tissues including cerebellum, midbrain, skeleton, and limbs (Loomis et al., 1996; Wurst et al., 1994). While EN1 expression persists in some cells such as mesencephalic dopaminergic neurons during adulthood, most other cell types silence the expression of EN1 after lineage commitment and do not express EN1 under homeostatic conditions in adulthood (Rekaik et al., 2015). However, a pathological environment can induce the expression of EN1 in these cells to promote phenotypical adaptation. In tissues from patients with triple-negative

[1]Department of Internal Medicine 3 - Rheumatology and Immunology, Friedrich-Alexander-University Erlangen-Nürnberg and University Hospital Erlangen, Erlangen, Germany; [2]Deutsches Zentrum für Immuntherapie, Friedrich-Alexander-University Erlangen-Nürnberg and University Hospital Erlangen, Erlangen, Germany; [3]Medical Informatics, Friedrich-Alexander University of Erlangen-Nürnberg, Erlangen, Germany; [4]Department of Rheumatology, Xiangya Hospital, Central South University, Changsha, Hunan, P.R. China; [5]Department of Plastic and Hand Surgery, Friedrich-Alexander-University Erlangen-Nürnberg and University Hospital Erlangen, Erlangen, Germany; [6]Department of Rheumatology, Center of Experimental Rheumatology, University Hospital of Zurich, Zurich, Switzerland; [7]State Key Laboratory of Genetic Engineering, Collaborative Innovation Center for Genetics and Development, School of Life Sciences, Fudan University, Shanghai, P.R. China; [8]Human Phenome Institute, Fudan University, Shanghai, P.R. China; [9]Institute of Rheumatology, Immunology and Allergy, Fudan University, Shanghai, P.R. China; [10]Department of Medicine II: Gastroenterology, Hepatology, Endocrinology, and Infectious Disease, University Medical Center Freiburg, Freiburg, Germany; [11]BIOSS Centre for Biological Signaling Studies, Freiburg, Germany.

*A.-H. Györfi and A.-E. Matei contributed equally to this work; Correspondence to Jörg H.W. Distler: joerg.distler@uk-erlangen.de.

breast cancer, for example, EN1 expression is up-regulated and correlates with poor patient survival; moreover, EN1 expression induces proliferation and migration of quintuple-negative breast cancer cells (Kim et al., 2018). Depending on the context, EN1 can regulate gene transcription either directly by binding to conserved EN1-binding sites in the promoters of target genes or indirectly by trans-activation or trans-repression by interacting with other transcription factors, with subsequent modulation of their transcriptional outcome (Alexandre and Vincent, 2003).

Of particular interest, En1 is transiently expressed during dermal development in murine embryos in a distinct fibroblast lineage (Rinkevich et al., 2015). In mice, En1-positive fibroblasts gradually replace En1-negative fibroblasts in the developing dermis (Jiang et al., 2018). The expression of En1, however, decreases rapidly before birth. Former EN1-positive cells give rise to a subpopulation of fibroblasts that has a high capacity for extracellular matrix (ECM) production and important roles in wound healing in adult murine skin (Jiang et al., 2018; Rinkevich et al., 2015). However, the regulation of EN1 in adult skin and its role in the pathological activation of fibroblasts in tissue fibrosis have not been studied thus far.

In this study, we show that TGFβ reactivates the expression of EN1 in a SMAD-dependent manner with increased numbers of EN1-positive fibroblasts in SSc skin. Imaging mass cytometry (IMC) of paired skin biopsies from SSc patients (from ventral and dorsal skin) show that EN1 is expressed by multiple fibroblast subpopulations in SSc. EN1 is a critical mediator of the profibrotic effects of TGFβ in adult fibroblasts: *EN1* overexpression in adult human dermal fibroblasts promotes fibroblast-to-myofibroblast transition and collagen release, whereas knockdown of *EN1* prevents TGFβ-induced fibroblast-to-myofibroblast transition. *EN1* knockdown induces global transcriptomic changes in TGFβ-stimulated fibroblasts, preventing induction of a profibrotic gene expression profile. EN1 trans-regulates gene expression by modulating the activity of transcription factors from the C2H2 zinc finger family, in particular those from the specificity protein (SP) subfamily. Chromatin immunoprecipitation followed by sequencing (ChIP-seq) experiments for both EN1 and SP1 demonstrate no direct binding of EN1 to the promoters of EN1-DEGs, but EN1-driven modulation of SP1 binding to the promoter of fibrosis-relevant genes. Mechanistically, changes of gene expression induced indirectly by *EN1* knockdown, in particular genes with predicted regulation by SP transcription factors and especially with SP1 binding, lead to stabilization of microtubules and reduced Rho-associated protein kinase (ROCK) activity, with subsequent prevention of TGFβ-induced stress fiber formation, myofibroblast transition, and fibrotic transformation of three-dimensional (3D) full-thickness skin equivalents. Consistently, fibroblast-specific *En1* knockout ameliorates dermal fibrosis in three complementary inflammation-driven and inflammation-independent mouse models of SSc. We thus characterize EN1 as a mediator of TGFβ-induced fibroblast activation and fibrosis.

Results

EN1 expression is up-regulated in fibrotic skin

We first analyzed the expression of different members of the EN family of homeodomain-containing transcription factors in the skin of patients with SSc. Immunofluorescence staining demonstrated increased expression of EN1 and prominent staining, with nucleocytoplasmic pattern, in dermal fibroblasts (identified as prolyl-4-hydroxylase-β [P4Hβ]–positive, CD45-negative cells) in the skin of SSc patients (Fig. 1 A). The percentage of EN1-positive fibroblasts was increased in SSc patients as compared with healthy individuals (Fig. 1 A). Other cell populations such as endothelial cells, leukocytes, and keratinocytes were stained with lower intensity for EN1 than fibroblasts, and EN1 expression was not changed in SSc skin in these cells (Fig. S1). Higher expression levels of EN1 were maintained in SSc fibroblasts for several passages in vitro. Cultured fibroblasts from SSc patients expressed higher levels of *EN1* mRNA and EN1 intracellular protein and secreted higher amounts of EN1 as compared with healthy dermal fibroblasts (Fig. 1, B and C). The expression of En1 was also up-regulated in murine models of skin fibrosis, with higher En1 protein levels in fibrotic mice as compared with nonfibrotic controls (Fig. 1, D and E). Moreover, the percentage of En1-positive fibroblasts (defined as $En1^+$, $Vimentin^+$, $CD45^-$ cells) was highly increased in the dermis of bleomycin-challenged mice and in the hypodermis of Tsk-1 mice in comparison with their respective controls (Fig. 1, F and G). In contrast to EN1, the other member of the EN family, EN2, was expressed at very low levels and did not differ between fibrotic and healthy human skin.

EN1 is expressed by multiple fibroblast subpopulations in both ventral and dorsal SSc skin

To evaluate whether EN1 expression is a common characteristic of all fibroblasts or whether it is rather restricted to a fibroblast subpopulation in SSc, we performed multiplexed IMC from paired biopsies from ventral and dorsal skin of SSc patients (Fig. 2 A). We designed and validated a 22-plex panel for IMC that comprises well-characterized fibroblast markers such as P4Hβ, platelet-derived growth factor receptor α (PDGFRα), αSMA, fibroblast activation protein (FAP), FSP-1, Thy1, DPP4, and Cdh-11, allowing simultaneous identification of multiple fibroblast subpopulations. We used image segmentation algorithms to generate cell masks (Fig. 2 A), which allowed extraction of high-dimensional single-cell data of marker expression. Subsequent clustering using the Phenograph algorithm identified 11 cellular clusters (Fig. 2 B). EN1 was expressed at various levels in all clusters, with the highest expression (>1 SD above the mean) in clusters 6 and 7 and the lowest expression in clusters 1 and 4 (Fig. 2, C and D). Clusters 6 and 7 also showed particularly high expression of αSMA as the typical myofibroblast marker (Fig. 2, D–H). Cluster 6 identifies a subpopulation with high expression of most fibroblast markers, but also of CD31/von Willebrand factor and with a particular perivascular localization, suggestive of cells that may have undergone endothelial-to-mesenchymal transition (Fig. 2, D–H). Other clusters that express EN1 at intermediate levels are characterized by marker expression of different fibroblast subpopulations: cluster 8 predominantly expresses Cdh-11; clusters 9 and 10 highly express FAP; and cluster 5 expresses FSP-1 (Fig. 2 D). EN1 expression was similar in dorsal and ventral skin, but clusters 6 and 7 were underrepresented and cluster 9 was nearly absent in

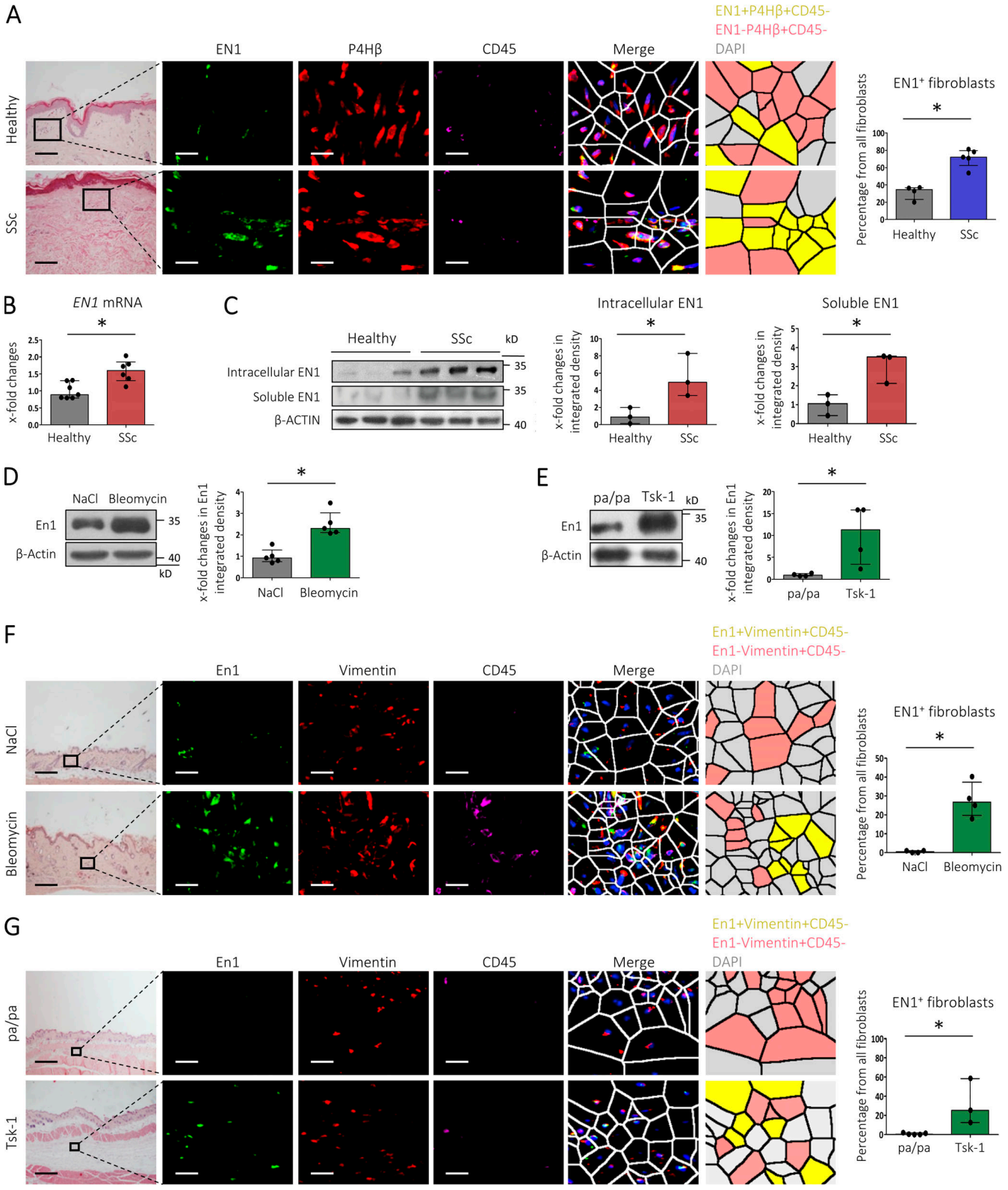

Figure 1. **EN1 expression is up-regulated in fibrotic skin. (A)** Representative immunofluorescence stainings for EN1 (green) and costainings with P4H (red) and CD45 (magenta) in the dermis of healthy donors and SSc patients at 1,000-fold magnification (scale bars = 20 µm). Hematoxylin and eosin stainings (200-fold magnification, scale bars = 100 µm), Voronoi diagrams, and percentages of EN1-positive fibroblasts from all fibroblasts (defined as $P4H^{+}CD45^{-}$ cells) are included. Data are shown from one experiment ($n \geq 4$). **(B and C)** *EN1* mRNA (B) and EN1 intracellular or secreted protein levels (C) in cultured fibroblasts or their supernatants from healthy donors and SSc patients. Representative Western blot images and quantifications are included (C). Data are shown from one experiment ($n = 3$). **(D and E)** En1 protein levels in the skin of mice challenged with bleomycin (D) or Tsk-1 mice (E) and their respective controls. Representative Western blot images and quantifications are included. Data are compiled from two independent experiments ($n \geq 4$). **(F and G)** Representative

immunofluorescence stainings for EN1 (green) and costainings with Vimentin (red) and CD45 (magenta) in the dermis of mice challenged with bleomycin and their controls at 1,000-fold magnification (F; scale bars = 20 µm) and in the hypodermis of Tsk-1 mice and their controls, respectively, at 1,000-fold magnification (G; scale bars = 20 µm). Hematoxylin and eosin stainings (100-fold magnification, scale bars = 200 µm [F] and 40-fold magnification, scale bars = 500 µm [G]), Voronoi diagrams, and percentages of EN1-positive fibroblasts from all fibroblasts (defined as Vimentin$^+$CD45$^-$ cells) are included. Data are shown from one experiment each ($n \geq 3$). All data are represented as median ± interquartile range. P values are expressed as follows: *, 0.05 > P > 0.01 (Mann-Whitney *U* test).

ventral skin (Fig. S1, D–F). In contrast, cluster 8, expressing EN1 at intermediate levels, was overrepresented in ventral skin (Fig. S1, D–F).

TGFβ signaling induces EN1 expression in a SMAD3-dependent manner

SSc fibroblasts are characterized by persistent up-regulation of TGFβ signaling under culture conditions. Considering the up-regulation of EN1 in cultured SSc fibroblasts, as well as in SSc patients and different mouse models of skin fibrosis, we hypothesized that TGFβ may reactivate the expression of EN1 in SSc skin. Indeed, stimulation of cultured fibroblasts with recombinant TGFβ induced a persistent up-regulation of EN1 protein levels (Fig. 3 A). In murine skin, activation of TGFβ signaling by overexpression of a constitutively active TGFβ receptor type I (TBRI^{CA}) increased the protein levels of En1 and induced the expression of En1 in dermal fibroblasts (Vimentin$^+$, CD45$^-$ cells; Fig. 3, B and C). Inhibition of TGFβ signaling by treatment with the selective TBRI inhibitor SD-208 prevented the up-regulation of En1 in bleomycin-induced skin fibrosis and in fibrotic skin of Tsk-1 mice, further highlighting that TGFβ is required for the up-regulation of En1 in fibrotic conditions (Fig. 3, D and E). The stimulatory effect of TGFβ on EN1 expression is SMAD3-dependent, as siRNA-mediated knockdown of *SMAD3* abrogated the induction of EN1 by TGFβ in vitro (Fig. 3 F). In vivo, inhibition of canonical TGFβ signaling by Smad3 siRNA prevented En1 up-regulation in the skin of TBRI^{CA}- and bleomycin-challenged mice, confirming the Smad3 dependence of the TGFβ-induced En1 up-regulation (Fig. 3, G and H). In silico analysis of the EN1 promoter revealed two SMAD3 binding sites. ChIP PCR confirmed enhanced binding of SMAD3 to both predicted SMAD3-binding sites in the EN1 promoter upon TGFβ stimulation (Fig. 3 I).

EN1 promotes fibroblast activation and collagen production

We next analyzed whether EN1 can regulate fibroblast activation. siRNA-mediated knockdown of *EN1* in adult human dermal fibroblasts rendered them less sensitive to the profibrotic effects of TGFβ, with lower levels of *COL1A1* and *COL1A2* mRNA, and reduced release of collagen protein (compared with non-targeting siRNA–treated fibroblasts; Fig. 4, A and B). Moreover, *EN1* knockdown prevented TGFβ-induced fibroblast-to-myofibroblast transition, with reduced levels of *ACTA2* mRNA and αSMA protein and impaired stress fiber formation (Fig. 4, C–E). *En1*$^{fl/fl}$ murine fibroblasts transduced with AdCre (*En1*-knockout fibroblasts) released less collagen and expressed lower levels of myofibroblast markers in response to TGFβ than AdLacZ-transduced controls (with unaltered expression of En1; Fig. S2). Overexpression of *EN1* in human fibroblasts fostered TGFβ-induced fibroblast activation with higher levels of *COL1A1* and *COL1A2* mRNA and collagen protein and increased levels of *ACTA2* mRNA and αSMA protein and enhanced formation of stress fibers (Fig. 4, F–J). *EN1* overexpression also enhanced the profibrotic effects of IL-11, IL-13, and connective tissue growth factor (CTGF) on deposition of fibronectin and collagen type I, expression of αSMA, and formation of stress fibers, but to a much lesser extent than the effects of TGFβ (Fig. S3).

EN1 induces a profibrotic profile of gene expression by modulation of SP binding to the promoters of profibrotic genes

To evaluate whether EN1 induces transcriptomic changes to promote fibroblast activation, we performed RNA sequencing (RNA-seq) from adult human dermal fibroblasts with knockdown of *EN1*. We identified 632 high-confidence differentially expressed genes (EN1-DEGs; 239 down-regulated and 315 up-regulated) between TGFβ-stimulated fibroblasts with siRNA-induced *EN1* knockdown and TGFβ-stimulated fibroblasts transfected with nontargeting siRNA (Fig. 5 A). gProfiler enrichment analysis of the EN1-DEGs revealed enrichment of multiple gene ontology (GO) and Reactome terms related to ECM production and organization (such as collagen formation or ECM organization), cytoskeleton organization (such as microtubule cytoskeleton organization or cytoskeleton), and Rho GTPases activity (such as signaling by Rho GTPases), confirming the functional relevance of EN1-regulated gene expression for TGFβ-induced fibroblast activation (Fig. 5 B). Gene set enrichment analysis (GSEA) revealed that EN1 expression levels did not influence apoptosis-related gene sets (Fig. 5 C).

We next performed in silico transcription factor profiling of the promoters of EN1-DEGs. We screened the promoter regions of all EN1-DEGs for potential binding sites against all available human transcription factor matrices (Table S4). Of note, we did not identify statistically enriched EN1-binding sites in EN1-DEGs (Table S4), indicating that EN1 may rather indirectly regulate gene expression in TGFβ-stimulated fibroblasts via modulation of the transcriptional activity of other transcription factors.

We found, in particular, members of the SP subfamily of C2H2 zinc finger transcription factors to be enriched in EN1-DEGs, with more than twofold increases of binding motifs for SP1, SP2, SP3, and SP8 as compared with the mean of two randomly generated gene sets as negative controls (Fig. S4 A). Coimmunoprecipitation experiments demonstrated that TGFβ promotes interaction of EN1 with SP1, providing experimental validation for the in silico model of EN1-mediated transcriptional regulation (Fig. 5 E). Although more common in up-regulated EN1-DEGs, SP1-, SP2-, SP3-, and SP8-binding motifs were present in the promoters of up- and down-regulated EN1-DEGs, suggesting that recruitment of additional transcriptional

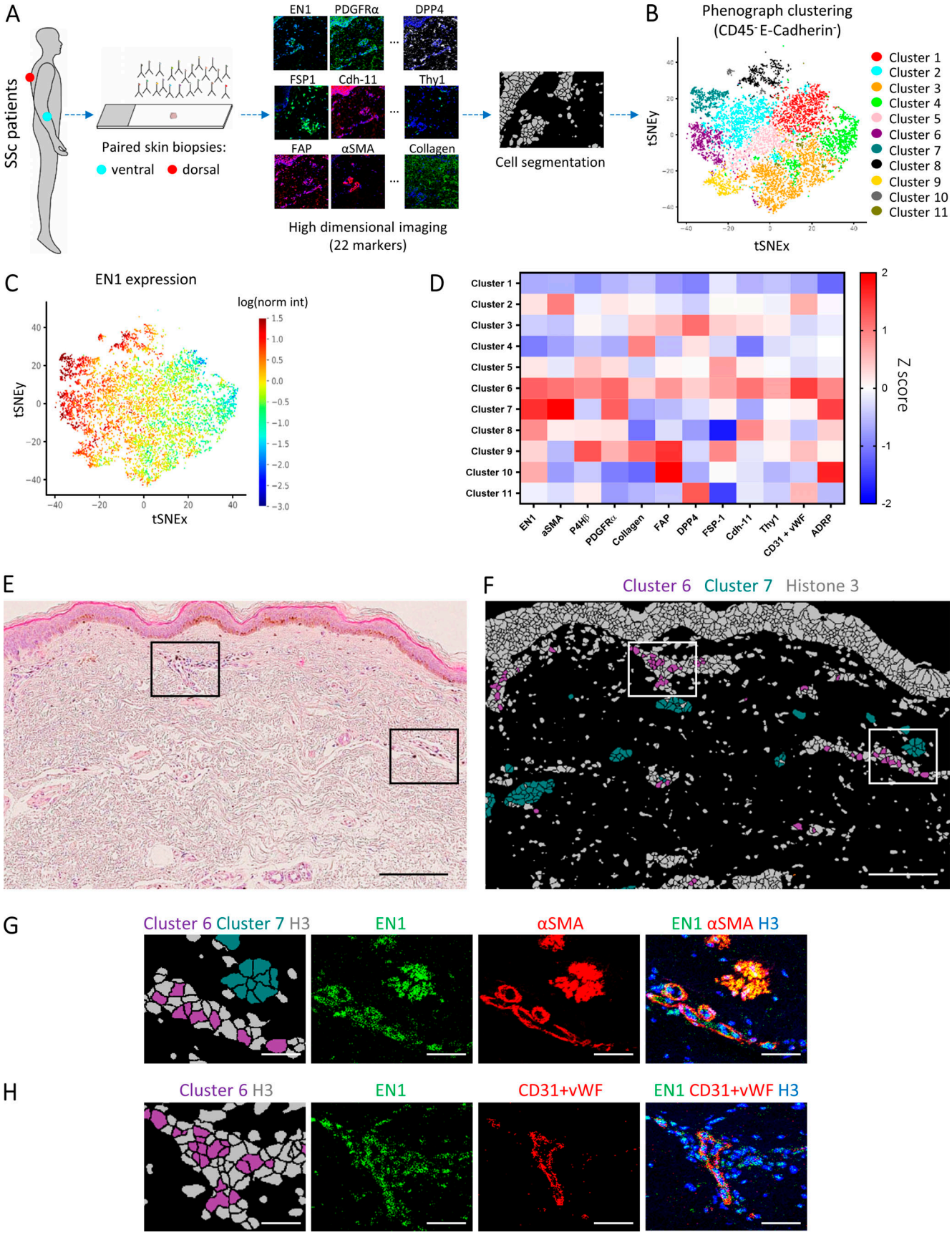

Figure 2. **EN1 is expressed in multiple fibroblast subpopulations in the skin of SSc patients. (A)** Schematic representation of the experimental and analytical workflow. IMC was performed on paired skin biopsies from ventral and dorsal skin from four SSc patients stained with a panel consisting of

22 metal-labeled antibodies. Segmentation of the multiplexed images comprising the signals from all markers into masks representing single cells was performed. **(B)** Phenograph clustering and visualization on a tSNE map of CD45⁻ E-Cadherin⁻ cells from all patients, regardless of biopsy location. **(C)** Expression of EN1 (as log[normalized intensity]) across the clusters. **(D)** Heatmap of marker expression across the clusters (as Z-score). **(E and F)** Representative hematoxylin and eosin staining (E) and schematic representation of clusters 6 and 7 (as the clusters with the highest expression of EN1, >1 SD above the mean; F), illustrating the spatial relationships of cells belonging to these clusters (scale bars = 200 µm). **(G and H)** Visualization of the area of interest marked in F, with EN1 signals (green) and αSMA (G) or CD31 and von Willebrand factor (H; red) as the markers with the highest expression from the clusters 6 and 7 (scale bars = 50 µm). Data were obtained from *n* = 8 biological samples from 4 SSc patients (paired ventral and dorsal biopsies) from one experiment.

regulators may determine the transcriptional outcome of EN1-SP1/2/3/8 binding (Fig. S4 A).

Further transcription factor coregulation analysis of the promoters of these EN1-DEGs with SP1-, SP2-, SP3-, and SP8-binding motifs (EN1-SP-DEGs) revealed a consistent pattern for all four SP members, with major enrichment of binding sites for other members of the C2H2 family (in particular, KLF5, 16, and 9 and ZNF263 and 384), as well as for members of the EF family (E2F4 and E2F6; Table S5). Binding sites for these transcription factors were found in similar frequencies in up- and down-regulated EN1-SP-DEGs (Fig. S4 B). Interestingly, we also identified binding motifs for other transcription factors that were exclusively present in up- or in down-regulated genes: binding motifs for transcription factor AP-2α (TFAP2A) were enriched in up-regulated EN1-SP-DEGs, indicating that in conditions of increased expression of EN1 recruitment of TFAP2A may promote transcriptional repression; in contrast, binding motifs for nuclear transcription factor Y β (NFYB) and for transcription factor Dp-1 (TFDP1) were exclusively found in down-regulated EN1-SP-DEGs (Fig. S4 B and Table S5), suggesting that their recruitment may promote transcriptional activation.

Functional analysis of the EN1-SP-DEGs and EN1-SP-DEGs with binding motifs for other C2H2 transcription factors revealed major enrichment of processes related to fibroblast activation, in particular of those pertaining to cytoskeleton organization and Rho GTPases activity (Fig. 5 D and Table S6).

EN1 ChIP-seq showed binding of EN1 predominantly to intergenic and intronic regions, while SP1 ChIP-seq revealed binding of SP1 predominantly to promoter regions in all three biological replicates (Fig. 6 A). SP1 ChIP-seq demonstrated that knockdown of *EN1* significantly decreases the genomic binding of SP1, with reduced peak counts and reduced activity of SP1 in peaks (Fig. 6, B and C). From the few genes with EN1 binding in promoter regions, only the following genes were shared among all three biological replicates: *ROCK1P1*, *DUX4*, and *PACSIN2*. Of note, all of these genes also showed binding of SP1 in their promoter region. We found no direct binding of EN1 to the promoters of EN1-DEGs; instead, we found binding of SP1 to the promoter of multiple EN1-DEGs, especially to the down-regulated EN1-DEGs. gProfiler enrichment analysis of the EN1-DEGs with direct binding of SP1 revealed enrichment of multiple GO and Reactome terms related to fibrosis such as cytoskeleton, microtubule, and signaling by Rho GTPases (Fig. 6 D).

EN1 promotes rearrangements of the microtubule-actin cytoskeleton in a ROCK-dependent manner to induce fibroblast activation

GSEA showed negative enrichment scores ("de-enrichment") for the GO gene sets regulation of actin nucleation and microtubule depolymerization in *EN1*-knockdown fibroblasts stimulated with TGFβ, suggesting that EN1 might induce myofibroblast differentiation by promoting microtubule-dependent cytoskeletal rearrangements (Fig. 7 A).

Microtubule depolymerization induces stress fiber assembly at focal adhesions and promotes cell contraction (Liu et al., 1998; Ng et al., 2014). To experimentally validate an EN1-dependent regulation of microtubules in fibroblasts, we analyzed the microtubule polymerization state in human dermal fibroblasts with overexpression or knockdown of *EN1* by two methods: Western blot for insoluble and soluble tubulin and a previously described tubulin polymerization high-content imaging assay (Sum et al., 2014). Overexpression of *EN1* promotes depolymerization of the microtubular network, with reduced tubulin intensity on immunofluorescence stainings and decreased insoluble/soluble tubulin ratio on Western blot (Fig. 7, B and C). In contrast, knockdown of *EN1* enhanced the formation of microtubular networks, with increased tubulin intensity and higher insoluble/soluble tubulin ratio (Fig. S5, A and B). Incubation with paclitaxel, a stabilizer of microtubules, phenocopied the stimulatory effects of *EN1* knockdown and prevented the inhibitory effects of *EN1* overexpression on microtubule polymerization (Fig. S5, A and B; and Fig. 7, B and C). In contrast, vinblastine, an inhibitor of microtubule polymerization, abrogated the stimulatory effects of *EN1* knockdown on microtubule elongation (Fig. S5, A and B).

We next tested whether EN1 might regulate stress fiber formation and myofibroblast differentiation by modulation of the microtubular network. Indeed, microtubule stabilization by paclitaxel abrogated myofibroblast differentiation induced by *EN1* overexpression, with reduced collagen production, αSMA expression, and stress fiber formation in fibroblasts from standard 2D culture (Fig. 7, D–H). Moreover, microtubule stabilization with paclitaxel prevented the profibrotic effects of EN1 on 3D full-thickness skin equivalents, with lower levels of *COL1A1* and *ACTA2* mRNA, decreased myofibroblast counts, and reduced thickening of the dermal portion of the skin equivalents compared with vehicle-treated controls (Fig. 9). In contrast, microtubule depolymerization by vinblastine abrogated the inhibitory effects of *EN1* knockdown on TGFβ-induced fibroblast-to-myofibroblast transition (Fig. S5, C–G).

De-enriched GO and Reactome terms also included signaling by Rho GTPases and Rho GTPase effectors (Fig. 8 A). The activity of Rho GTPases and of one of their downstream effectors, ROCK, plays a critical role in regulation of the cytoskeleton (Chang et al., 2008; Krendel et al., 2002). We thus hypothesized that EN1 may induce ROCK activity by depolymerizing microtubules to promote stress fiber assembly and fibroblast activation. Indeed, knockdown of *EN1* prevented the stimulatory effects of TGFβ on ROCK activity, whereas overexpression of *EN1* increased

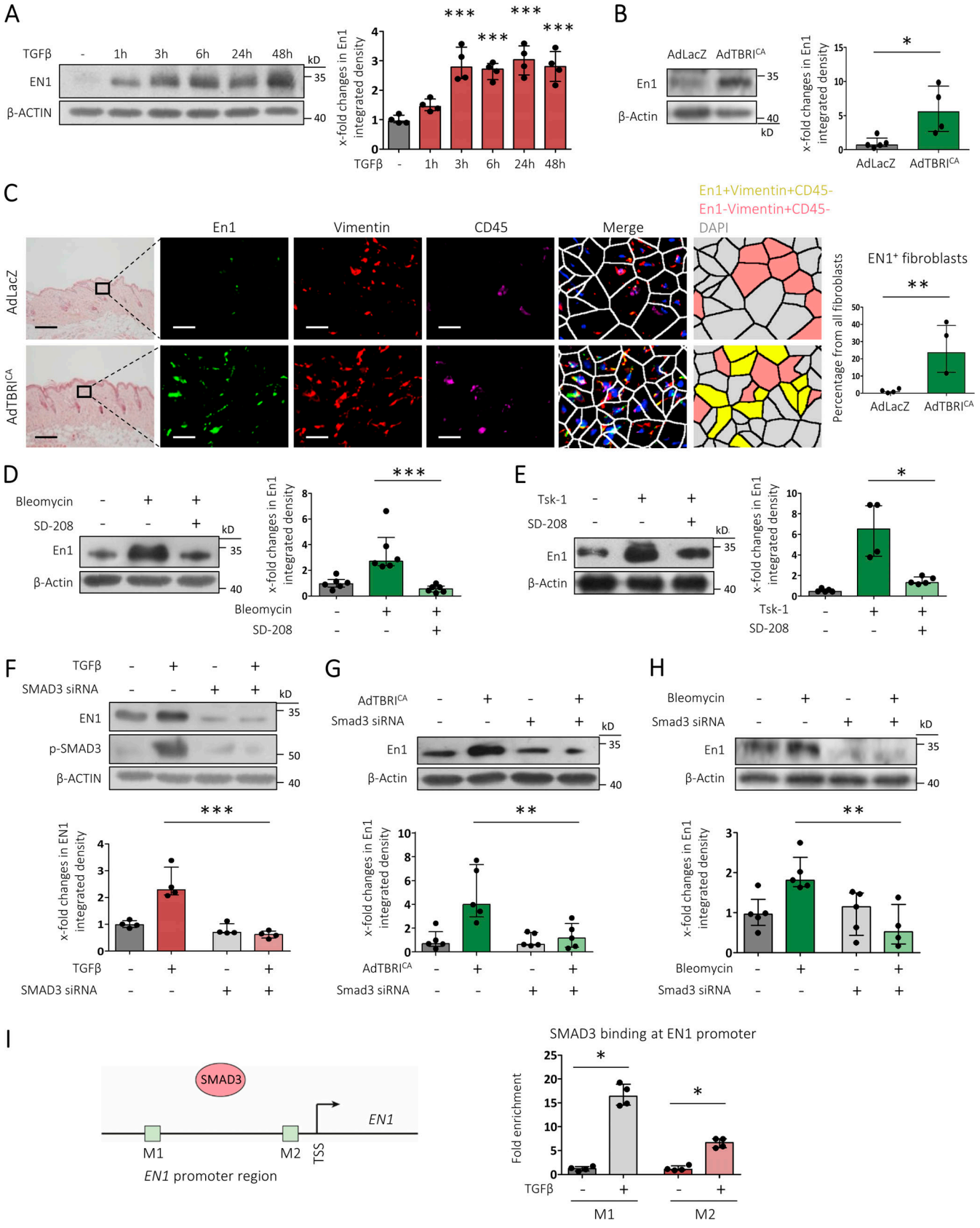

Figure 3. **TGFβ up-regulates EN1 in a SMAD3-dependent manner. (A)** EN1 protein levels in cultured human fibroblasts at 1, 3, 6, 24, and 48 h after TGFβ stimulation. Representative Western blot images and quantification are included. Data are compiled from two experiments ($n \geq 4$). **(B)** En1 protein levels in the skin of mice expressing TBRI^{CA} and their controls. Representative Western blot images and quantifications are included. Data are compiled from two

experiments ($n \geq 4$). **(C)** Representative immunofluorescence stainings for En1 (green) and costainings with Vimentin (red) and CD45 (magenta) in the dermis of mice expressing $TBRI^{CA}$ and their controls at 1,000-fold magnification (scale bars = 20 µm). Data are shown from one experiment ($n \geq 4$). Hematoxylin and eosin stainings (100-fold magnification, scale bars = 200 µm), Voronoi diagrams, and percentages of EN1-positive fibroblasts from all fibroblasts (defined as $Vimentin^{+}CD45^{-}$ cells) are included. **(D and E)** En1 protein levels in the skin of mice challenged with bleomycin (D) or Tsk-1 mice (E) and/or treated with the TBRI inhibitor SD-208 and their respective controls. Representative Western blot images and quantifications are included. Data are compiled from two experiments ($n \geq 4$). **(F)** EN1 protein levels in cultured human fibroblasts with siRNA-mediated *SMAD3* knockdown with or without stimulation with TGFβ (24 h) and their controls (fibroblasts transfected with nontargeting siRNA). Representative Western blot images and quantification are included. Data are compiled from two experiments ($n = 4$). **(G and H)** En1 protein levels in the skin of $TBRI^{CA}$ mice (or, as controls, mice injected with an adenovirus expressing LacZ; G) or of mice challenged with bleomycin (or, as controls, mice injected with NaCl; H) and/or treated with SMAD3 siRNA and their controls (mice injected with nontargeting siRNA). Representative Western blot images and quantifications are included. Data are compiled from two experiments ($n = 5$). **(I)** ChIP PCR for SMAD3 binding at predicted SMAD3 motifs in the promoter of EN1. Data are compiled from two experiments ($n = 4$). All data are represented as median ± interquartile range. P values are expressed as follows: *, $0.05 > P > 0.01$; **, $0.01 > P > 0.001$; ***, $P < 0.001$ (Mann–Whitney *U* test for B and C; ANOVA with Tukey's post hoc test for A and D–I).

ROCK activity at baseline and in response to TGFβ (Fig. 8, B and C). Stabilization of microtubules with paclitaxel prevented the induction of ROCK activity by EN1, highlighting that microtubule depolymerization is required for EN1 to induce ROCK activity (Fig. 8 C). Moreover, the selective ROCK inhibitor Y27632 prevented EN1-induced myofibroblast differentiation, stress fiber formation, and fibrotic transformation of 3D full-thickness skin equivalents (Fig. 8, D–H; and Fig. 9). Thus, EN1 promotes depolymerization of microtubules to induce ROCK activity, which facilitates TGFβ-induced stress fiber formation, myofibroblast differentiation, and collagen deposition.

Knockout of *En1* ameliorates experimental skin fibrosis

To analyze whether knockout of *En1* reduces fibroblast activation in vivo and protects from experimental fibrosis, we generated $En1^{fl/fl}$ × *Col6Cre* mice, with fibroblast-specific constitutive *En1* knockout. Mice with selective depletion of En1 in fibroblasts did not show a basic phenotype in the absence of profibrotic stimuli as compared with controls, and their dermal structure was preserved (Fig. 10). We employed three complementary models of skin fibrosis: (1) the $TBRI^{CA}$ model; (2) the bleomycin-induced model; and (3) the Tsk-1 model. Skin fibrosis was strongly ameliorated in mice with fibroblast-specific knockout of *En1* in comparison with control mice in all three models, with reduced dermal or hypodermal thickness, lower myofibroblast counts, and reduced hydroxyproline content (Fig. 10, A–L).

Discussion

A landmark study by Rinkevich et al. (2015) and a follow up study by Jiang et al. (2018) showed that a subpopulation of fibroblasts transiently express En1 during skin development in murine embryos. The number of En1-positive fibroblasts increases during embryonic development, but these cells silence the expression of En1 before birth under homeostatic conditions (Jiang et al., 2018). However, the regulation of En1 expression was not investigated in these studies. Here, we demonstrate that EN1 expression is up-regulated in fibrotic skin of SSc patients compared with skin from healthy donors, as well as in three different murine models of skin fibrosis. Multiple fibroblast subpopulations express EN1 in adult skin of SSc patients, in particular fibroblast subpopulations with high expression of αSMA. A previous study evaluated the expression of EN1 in adult human skin by immunohistochemistry (Miura et al., 2018). Although not specifically followed up by the authors, EN1-positive single cells can be observed in the dermis, suggesting that, in line with our results, adult fibroblasts in human skin can express EN1. In contrast to the redundant expression of EN1 and EN2 in dopaminergic neurons (Hanks et al., 1995), the low expression of EN2 in adult skin and the lack of induction in fibrotic skin excluded a major role of EN2 in skin fibrosis.

We demonstrate on multiple experimental levels that canonical TGFβ signaling reactivates the expression of EN1 in cultured fibroblasts and fibrotic skin. (1) Stimulation of cultured dermal fibroblasts with recombinant TGFβ up-regulates the intracellular levels of EN1. (2) EN1 levels are increased in SSc fibroblasts as compared with fibroblasts isolated from healthy individuals even after several passages in culture. As persistent activation of TGFβ signaling is a major characteristic of SSc fibroblasts, this finding provides indirect evidence for a TGFβ-dependent regulation of EN1 in SSc. (3) Overexpression of $TBRI^{CA}$ increases En1 protein levels in murine skin, thus confirming that TGFβ is sufficient to increase the expression levels of En1 in fibroblasts in vivo. (4) The induction of EN1 by TGFβ is mediated by canonical TGFβ/SMAD3 signaling, as knockdown of *SMAD3* abrogates the stimulatory effects of TGFβ on EN1 expression in cultured fibroblasts and in murine skin. (5) Selective inhibition of TGFβ signaling prevented the up-regulation of En1 in bleomycin-induced and Tsk-1 models of experimental skin fibrosis, highlighting that TGFβ signaling is essentially required for the up-regulation of En1 in fibrotic skin.

However, additional factors other than TGFβ may also promote the expression of EN1. EN1 has been shown to be a target of WNT1 in vertebrate midbrain development, and WNT1 is also up-regulated in multiple fibrotic disorders including SSc (Akhmetshina et al., 2012; Bergmann and Distler, 2016; Beyer et al., 2012b; Danielian and McMahon, 1996; Königshoff et al., 2009). Notch signaling, another stem cell pathway that is hyperactive in SSc, is required to maintain the expression of engrailed during the development of the ocellar complex in *Drosophila melanogaster* (Aguilar-Hidalgo et al., 2013; Beyer and Distler, 2013; Dees et al., 2011a; Dees et al., 2011b). Finally, ischemia-reperfusion injury, which may occur as a consequence of microvascular endothelial dysfunction in SSc, can also induce EN1 expression and may contribute to its up-regulation in SSc (Beyer et al., 2009; Villanueva et al., 2006).

In extension of the findings by Rinkevich et al. (2015), we demonstrate that EN1 not only serves as an embryonic marker

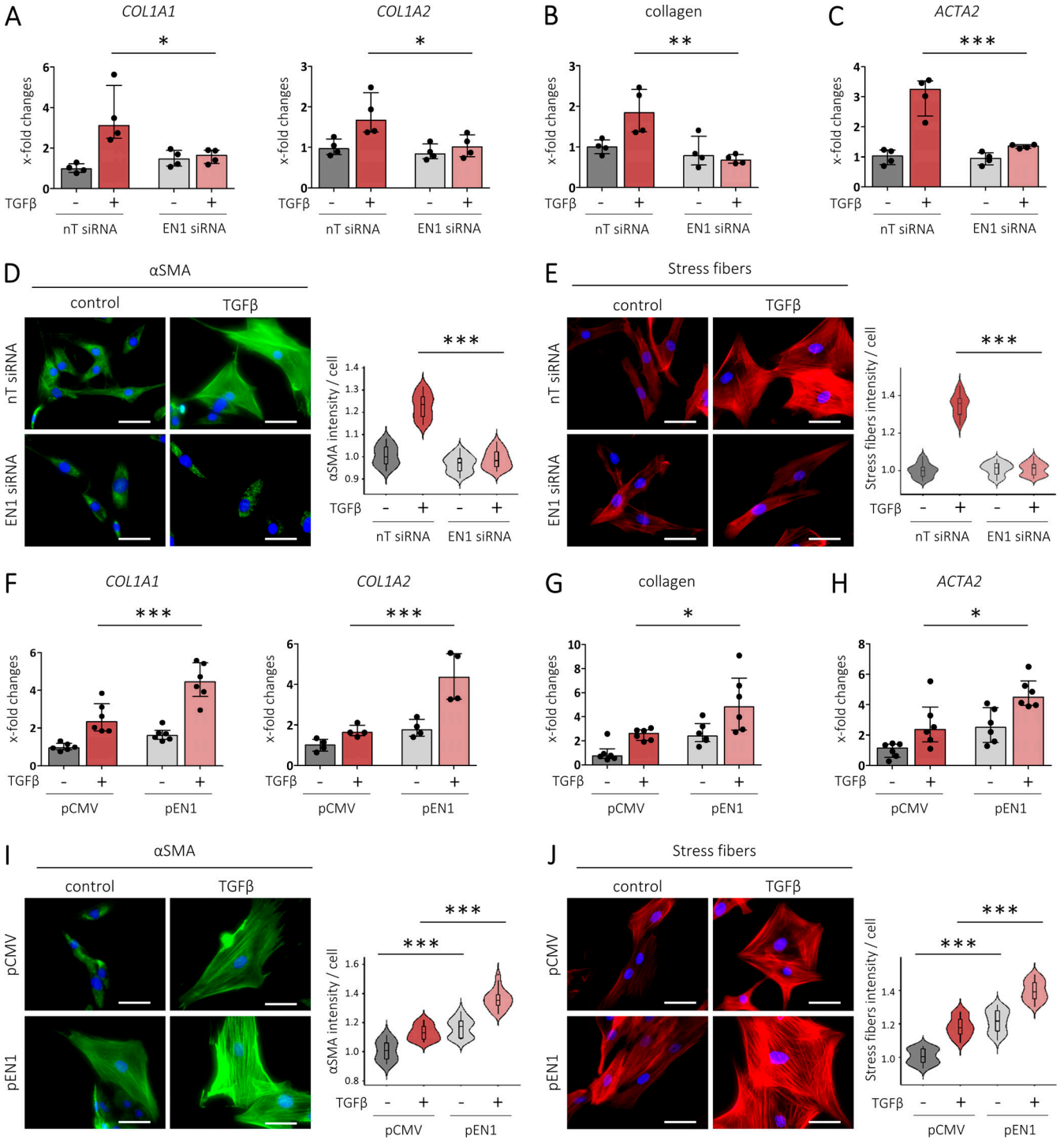

Figure 4. **EN1 promotes fibroblast activation and collagen production. (A–E)** siRNA-mediated knockdown of *EN1* prevents TGFβ-induced fibroblast activation. Relative mRNA levels of *COL1A1* and *COL1A2* (A). Relative protein levels of secreted collagen type I (B). Relative mRNA levels of *ACTA2* (C). Representative immunofluorescence stainings for αSMA (D) and stress fibers (E) at 400-fold magnification (scale bars = 50 µm). Quantification of average signal intensity for each cell (relative to control) is included. Data for A–E were obtained from $n \geq 4$ independent biological samples per group from two independent experiments. **(F–J)** *EN1* overexpression promotes fibroblast activation. Relative mRNA levels of *COL1A1* and *COL1A2* (F). Relative protein levels of secreted collagen type I (G). Relative mRNA levels of *ACTA2* (H). Data for F–J were obtained from $n \geq 4$ independent biological samples per group from two independent experiments. Representative immunofluorescence stainings for αSMA (I) and stress fibers (J) at 400-fold magnification (scale bars = 50 µm). Quantification of average signal intensity for each cell (relative to control) is included. All data are represented as median ± interquartile range. P values are expressed as follows: *, 0.05 > P > 0.01; **, 0.01 > P > 0.001; ***, P < 0.001 (ANOVA with Tukey's post hoc test).

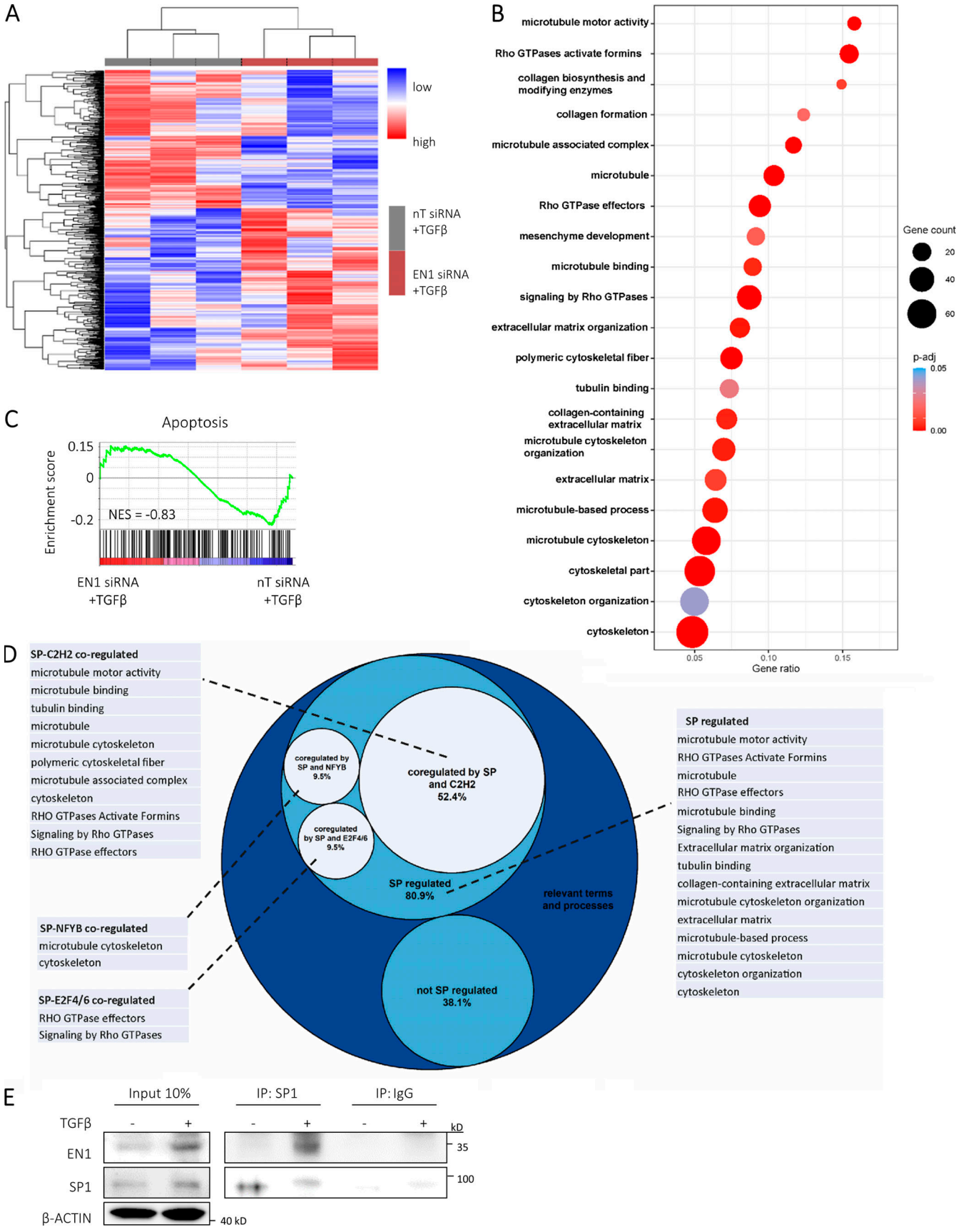

Figure 5. **EN1 induces a profibrotic gene expression profile. (A–C)** RNA-seq results showing that knockdown of *EN1* partially reverses the profibrotic gene expression profile induced by TGFβ, without affecting apoptosis. Heatmap of expression levels of the 632 EN1-DEGs across the three replicates for each

condition. Hierarchical clustering of the replicates and of the EN1-DEGs' expression are included (A). Dot plot showing gene ratio (on the x axis), gene count (as dot size), and adjusted P value (as color gradient) of selected enriched GO and Reactome terms (after g:Profiler enrichment analysis) related to fibrosis (B). GSEA of the apoptosis Reactome term (C). Data for A–C were obtained from $n = 3$ independent biological samples per group. **(D)** Circular packing plots illustrating enrichment of fibrosis-related GO and Reactome terms (after g:Profiler enrichment analysis) of the EN1-DEGs with predicted binding motifs for SP1/2/3/8 (SP) and cobinding with other members of the C2H2 or E2F families, or with NFYB (expressed as percentages from the total fibrosis-related processes enriched in EN1-DEGs). The threshold for DEGs was false discovery rate < 0.25 and fold-change >1.5, and the conditions were as follows: nontargeting siRNA treated human fibroblasts stimulated with TGFβ as reference group and EN1 siRNA treated human fibroblasts stimulated with TGFβ as treatment group. **(E)** Coimmunoprecipitation of EN1 with SP1 in human fibroblasts ± TGFβ (24 h). Representative Western blot images are included. Data were obtained from two independent experiments ($n = 3$).

for a defined population of fibroblasts with a high capacity to produce ECM proteins, but EN1 also regulates the activation status of adult human dermal fibroblasts. EN1-deficient fibroblasts are less sensitive to TGFβ-induced activation, whereas forced overexpression of *EN1* renders fibroblasts more susceptible to the profibrotic effects of TGFβ and, to a lesser extent, to those of other profibrotic molecules such as IL-11, IL-13, and CTGF (Ng et al., 2019; Schafer et al., 2017), with increased myofibroblast differentiation and enhanced collagen release. Moreover, *EN1* overexpression induces myofibroblast differentiation in the absence of external profibrotic stimuli. EN1 is thus both necessary to fully mount the fibroblast response to profibrotic stimuli (in particular to TGFβ) and also sufficient to induce fibroblast activation in the absence of external stimuli.

Selective depletion of En1 in fibroblasts also reduced the profibrotic effects of TGFβ signaling in vivo. Mice with fibroblast-specific knockout of *En1* were protected from experimental fibrosis induced by overexpression of a constitutively active TGFβ receptor type I. Fibroblast-specific depletion of En1 also ameliorated skin fibrosis in Tsk-1 mice and mice challenged with bleomycin. Lineage commitment of En1-expressing fibroblasts seemed to be unaffected in mice with fibroblast-specific *En1* knockout, since the structure and collagen composition of their dermis were comparable to those of littermates with unaltered En1 expression. Although the frequency of recombination in *Col6Cre* transgenic mice is almost absent in nonmesenchymal cells (Armaka et al., 2008), *Col6Cre*-induced recombination is less specific to fibroblasts than in, for example, *PDGFRα-Cre* (Horikawa et al., 2015). Despite this limitation of our study, the strong in vitro effects on fibroblast activation suggest that EN1 upregulation and aberrant signaling in fibroblasts play a pivotal role in skin fibrosis.

RNA-seq of adult human dermal fibroblasts with siRNA-mediated knockdown of *EN1* combined with functional experiments demonstrated that EN1 induces depolymerization of microtubules with a decreased ratio of insoluble to soluble tubulin. Disruption of the microtubule network promotes formation and maturation of focal adhesions in a ROCK-dependent manner, stimulating the assembly of actin stress fibers (Bershadsky et al., 1996; Liu et al., 1998; Ng et al., 2014), which is required to promote fibroblast-to-myofibroblast differentiation (Dugina et al., 2001; Hinz et al., 2003). Pharmacologic stabilization of microtubules or inhibition of ROCK prevents EN1-induced fibroblast-to-myofibroblast transition and collagen release in both standard 2D fibroblast cultures and 3D full-thickness skin equivalents. In contrast, pharmacologically induced microtubule depolymerization abrogates the antifibrotic effects of *EN1* knockdown. These data unravel a novel mechanism of regulation of cytoskeletal organization during fibroblast-to-myofibroblast differentiation in fibrotic diseases.

Mechanistically, the effects of EN1 on cytoskeleton and ROCK activity are not mediated by direct binding to EN1 motifs in EN1-DEGs, but by trans-regulation, i.e., by modulating the activity/binding of SP family members of transcription factors. ChIP-seq experiments for EN1 and SP1, the SP member with the most predicted binding motifs in the EN1-DEGs, showed that EN1 predominantly binds to intergenic and intronic regions, while SP1 predominantly binds to promoter regions. Our results are in line with previous EN1 ChIP-seq data from triple-negative breast cancers, which also demonstrate predominant binding of EN1 to noncoding regions (Peluffo et al., 2019). ChIP-seq for EN1 supports the conclusion that EN1 regulates the binding of SP1 to the promoter of profibrotic genes related to the microtubule cytoskeleton and Rho GTPases. In silico transcription factor profiling suggests that the profibrotic roles of EN1 are likely mediated by interference with a network of profibrotic transcription factors including SP1 (validated by SP1 ChIP-seq), SP2, SP3, SP8, and other members of the C2H2 family (Córdova et al., 2015; Jiang et al., 2013; Manabe et al., 2002; Sysa et al., 2009; Verrecchia et al., 2001). The potent antifibrotic effects of *EN1* knockdown might thus be attributed to the cumulative changes in target specificity of multiple transcription factors.

In silico transcription factor profiling and functional enrichment analysis support an EN1-transcriptional regulation of gene expression with specific functional modularity: EN1-DEGs with predicted transcriptional regulation by SP family members (and coregulation by other members of the C2H2 family) are functionally related to fibroblast activation (in particular to cytoskeleton organization and Rho GTPases activity). These data implicate that EN1 can direct the specificity of SP-containing regulatory modules toward genes with functional relevance for fibrosis. Reducing EN1 levels or inhibiting the interaction of EN1 with SP family members may thus interfere with this pathological regulation of gene expression and reestablish the physiological target specificity of SP transcription factors.

Targeted inactivation of EN1, for instance with recently described synthetically designed EN1 interference peptides (EN1-iPep; Beltran et al., 2014; Gandhi et al., 2018; Sorolla et al., 2019) might thus offer therapeutic potential for the treatment of fibrotic diseases such as SSc. Considering the antiapoptotic roles of EN1 in dopaminergic neurons (Rekaik et al., 2015), a systemic therapy that targets EN1 may have adverse effects on the central nervous system. However, in the case of EN1-iPep, occurrence of

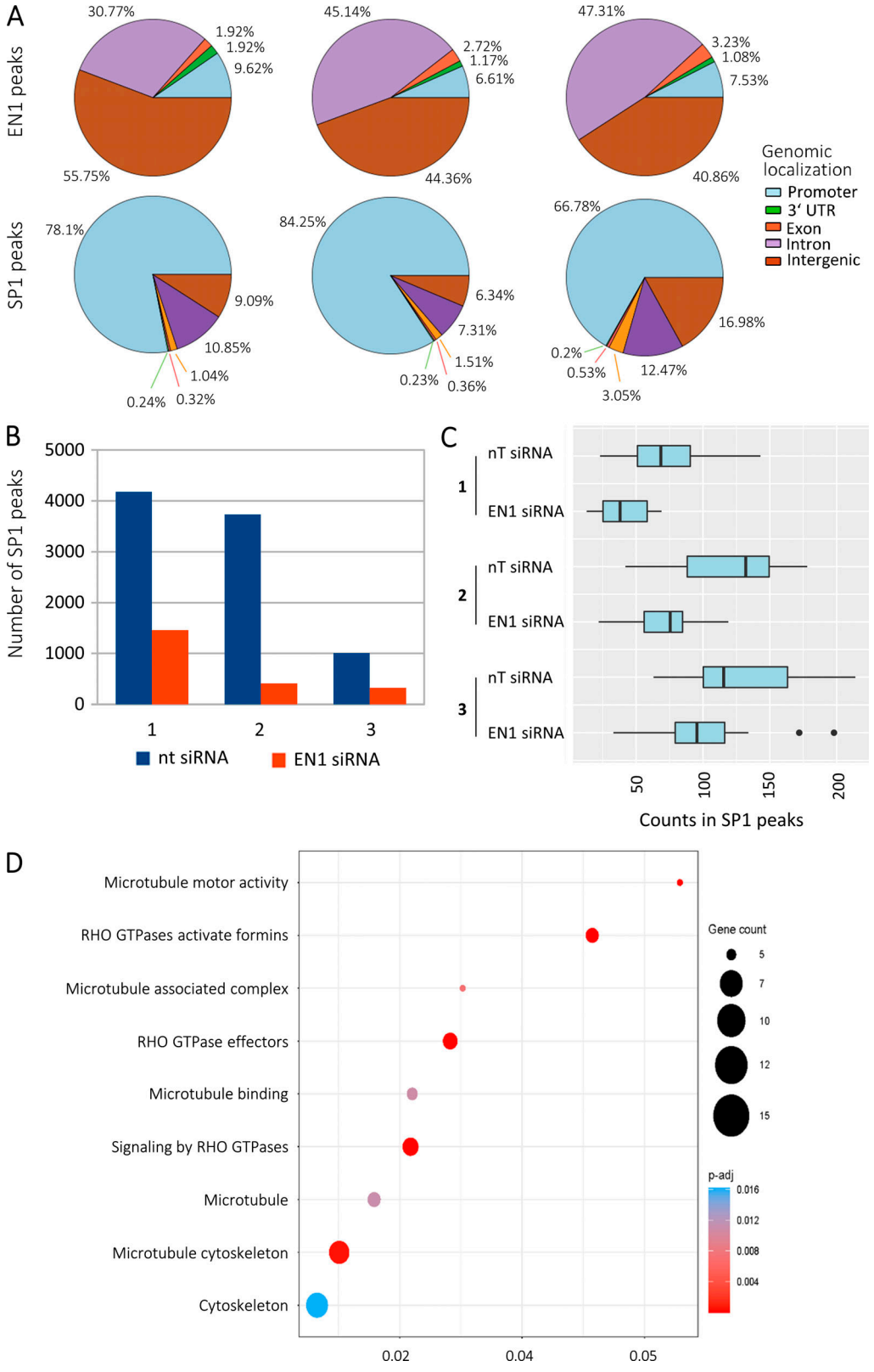

Figure 6. **Direct genomic targets of EN1 and SP1. (A)** Genomic localization of EN1 and SP1 peaks showing enrichment of EN1 peaks in intergenic and intronic regions, while SP1 peaks show great enrichment in promoter regions defined as 300–3,000 bp upstream from transcription start site. **(B and C)** Knockdown of *EN1* reduces the number and activity of SP1 peaks across all three biological replicates. Number of SP1 peaks (B). Read counts in SP1 peaks (C). **(D)** Dot plot showing gene ratio (on the x axis), gene count (as dot size), and adjusted P value (as color gradient) of selected enriched GO and Reactome terms after g:Profiler enrichment analysis of the EN1-DEGs with direct SP1 binding related to fibrosis. Data were obtained from $n = 3$ independent biological samples per group.

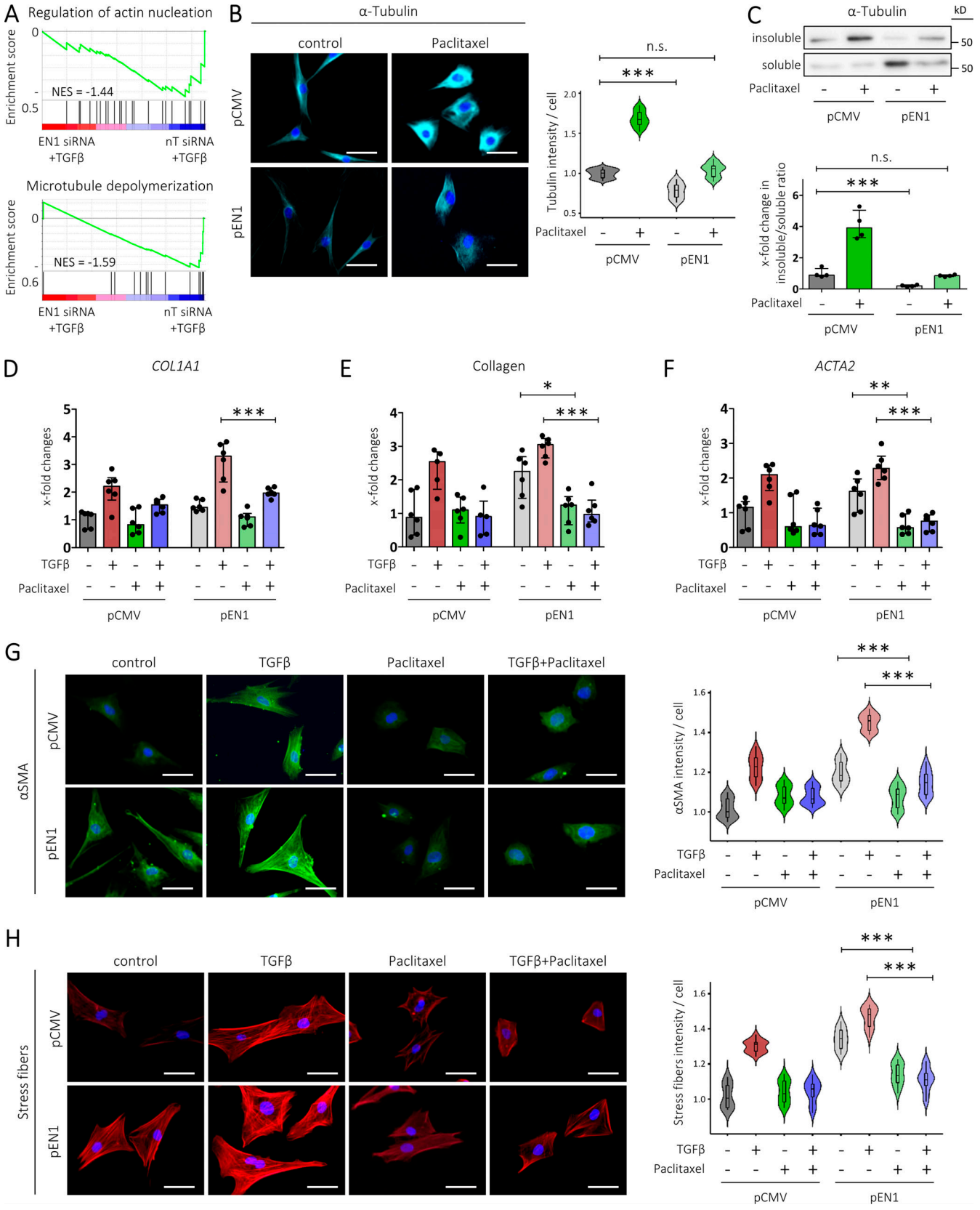

Figure 7. ***EN1* overexpression promotes microtubule depolymerization to induce myofibroblast differentiation. (A)** GSEA of the indicated GO terms, showing that *EN1* knockdown de-enriches genes related to microtubule depolymerization and actin nucleation. **(B and C)** *EN1* overexpression induces microtubule depolymerization. Representative immunofluorescence stainings for α-Tubulin at 400-fold magnification (scale bars = 50 µm). Quantification of total signal intensity for each cell (relative to control) is included (B). Protein levels of soluble and insoluble α-Tubulin. Representative Western blot images and

quantification of insoluble/soluble α-Tubulin ratio are included (C). Data for B and C were obtained from two independent experiments ($n \geq 4$). **(D–H)** Pharmacological stabilization of microtubules prevents EN1-induced myofibroblast differentiation. Relative mRNA levels of *COL1A1* (D). Relative protein levels of secreted collagen type I (E). Relative mRNA levels of *ACTA2* (F). Representative immunofluorescence stainings for αSMA (G) and stress fibers (H) at 400-fold magnification (scale bars = 50 µm). Quantification of average signal intensity for each cell (relative to control) is included. Data for D–H were obtained from two independent experiments ($n \geq 4$). All data are represented as median ± interquartile range. P values are expressed as follows: *, 0.05 > P > 0.01; **, 0.01 > P > 0.001; ***, P < 0.001 (ANOVA with Tukey's post hoc test).

major nervous system toxicity should be hindered by several factors: (1) the low diffusibility of EN1-iPep through the blood–brain barrier; (2) the C-terminal RGD domain of EN1-iPep (Sorolla et al., 2019) that increases the specificity for cells with high expression of integrin αv, such as fibroblasts (Margadant and Sonnenberg, 2010); and (3) the selective targeting of EN1, since EN2 can functionally substitute EN1 in the dopaminergic neurons. However, further studies would be required to test the efficacy and safety of targeting EN1 in fibrotic diseases.

In summary, we demonstrate that EN1, beyond its function as an embryonic marker for a population of metabolically active fibroblasts during embryonic development, is also expressed by multiple fibroblast subpopulations in the skin of SSc patients and functionally regulates fibroblast-to-myofibroblast transition in adult skin. EN1 interacts with SP1 (and presumably other members of the SP/C2H2 family of transcription factors) upon stimulation with TGFβ and enhances its binding to the promoter of profibrotic genes related to the microtubule cytoskeleton and Rho GTPases to promote depolymerization of microtubules. This induces stress fiber formation, myofibroblast differentiation, and collagen release in a ROCK-dependent manner. In contrast, EN1-deficient fibroblasts are less sensitive to the profibrotic effects of TGFβ. Moreover, fibroblast-specific knockout of *En1* ameliorates experimental skin fibrosis in several complementary models. As EN1 is up-regulated in fibrotic diseases in a TGFβ-dependent manner, it functions as a molecular amplifier of TGFβ signaling and TGFβ-induced fibroblast differentiation. Targeted inactivation of EN1 may thus offer potential to inhibit TGFβ signaling and fibroblast activation in fibrotic diseases.

Materials and methods

Patient samples

Skin biopsies from 10 SSc patients and 10 age- and sex-matched healthy volunteers were used for staining or fibroblast isolation. Skin biopsies from SSc patients were taken from the affected skin of the forearm. All patients fulfilled the American College of Rheumatology/European League Against Rheumatism 2013 criteria (van den Hoogen et al., 2013). Seven patients were female, and three were male. The median age of SSc patients was 44 yr (range 19–65), and median disease duration was 5 yr (range 1–12). Further clinical data are provided in Table S2. The human studies were approved by the ethics committee of the Medical Faculty of the University of Erlangen-Nuremberg. All patients and controls signed a consent form approved by the local institutional review board.

Animal studies

Mice carrying two conditional alleles of *En1* (*En1*$^{fl/fl}$), *En1*$^{tm8.1Alj}$/J (stock no. #007918, The Jackson Laboratory; Sgaier et al., 2007), were crossbred with *Col6Cre* mice, B6.Cg-Tg(Col6a1-cre)1Gkl/Flmg (obtained from G. Kollias, Institute of Immunology, Biomedical Sciences Research Center "Alexander Fleming," Vari, Greece; Armaka et al., 2008). For all mouse experiments, for *En1*$^{fl/fl}$ × *Col6Cre* mice with fibroblast-specific knockout of *En1*, *En1*$^{fl/fl}$ × *wt/wt* littermates without Cre-mediated recombination were used as controls. The role of EN1 signaling in fibrosis was investigated in three different mouse models: (1) In the model of bleomycin-induced dermal fibrosis, fibrosis was induced by subcutaneous injections of bleomycin (50 µg) every other day for 4 wk starting at age 6 wk (Dees et al., 2015; Soare et al., 2016). Littermates injected with 0.9% NaCl served as controls. (2) In the TBRI^{CA} skin fibrosis model, fibrosis was induced by subcutaneous injections of replication-deficient type 5 adenoviruses (6.67×10^7 viral particles/administration/mouse) encoding for a constitutively active TBRI construct every second week (Beyer et al., 2010). Fibrosis was evaluated after 8 wk. Mice injected with type 5 adenoviruses encoding for *LacZ* served as controls. (3) Tsk-1 mice are a genetic model of skin fibrosis with progressive accumulation of ECM in the hypodermal layer of the skin (Beyer et al., 2010). Tsk-1 mice, B6.Cg-*Fbn1*^{Tsk}/J (stock no. #014632, The Jackson Laboratory; Siracusa et al., 1996) were analyzed at an age of 10 wk (Beyer et al., 2012a). *En1*$^{fl/fl}$ × *Col6Cre* × wt/wt littermates were used as healthy controls. All animal experiments were approved by the government of Unterfranken in Würzburg, Germany.

Histological analyses

Skin sections were stained with hematoxylin and eosin or trichrome. Dermal or hypodermal thickness was analyzed in three consecutive skin sections from each mouse at four different sites/section in a blinded manner, as described (Akhmetshina et al., 2012). Pictures were taken at 40- or 100-fold magnification with a Nikon Eclipse 80i microscope. Immunohistochemistry staining using αSMA antibody (1:1,000, #A5228; Sigma-Aldrich) and goat anti-mouse HRP-conjugated secondary antibody (1:5,000, #P0447; Dako) was performed for the visualization and quantification of myofibroblast numbers in murine skin.

Cell culture

Human and murine fibroblasts were isolated and cultured as described previously (Chakraborty et al., 2017; Palumbo-Zerr et al., 2015). In healthy human dermal fibroblasts, *EN1* overexpression was induced by transfection of 0.5 µg of plasmid encoding the human *EN1* (Origene). Knockdown of *EN1* or of *SMAD3* was induced by transfection of 3 µg of *EN1*-targeting or *SMAD3*-targeting siRNA using an Amaxa 4D-Nucleofector. Healthy dermal fibroblasts transfected with an equal amount of empty vector or nontargeting siRNA served as controls. In

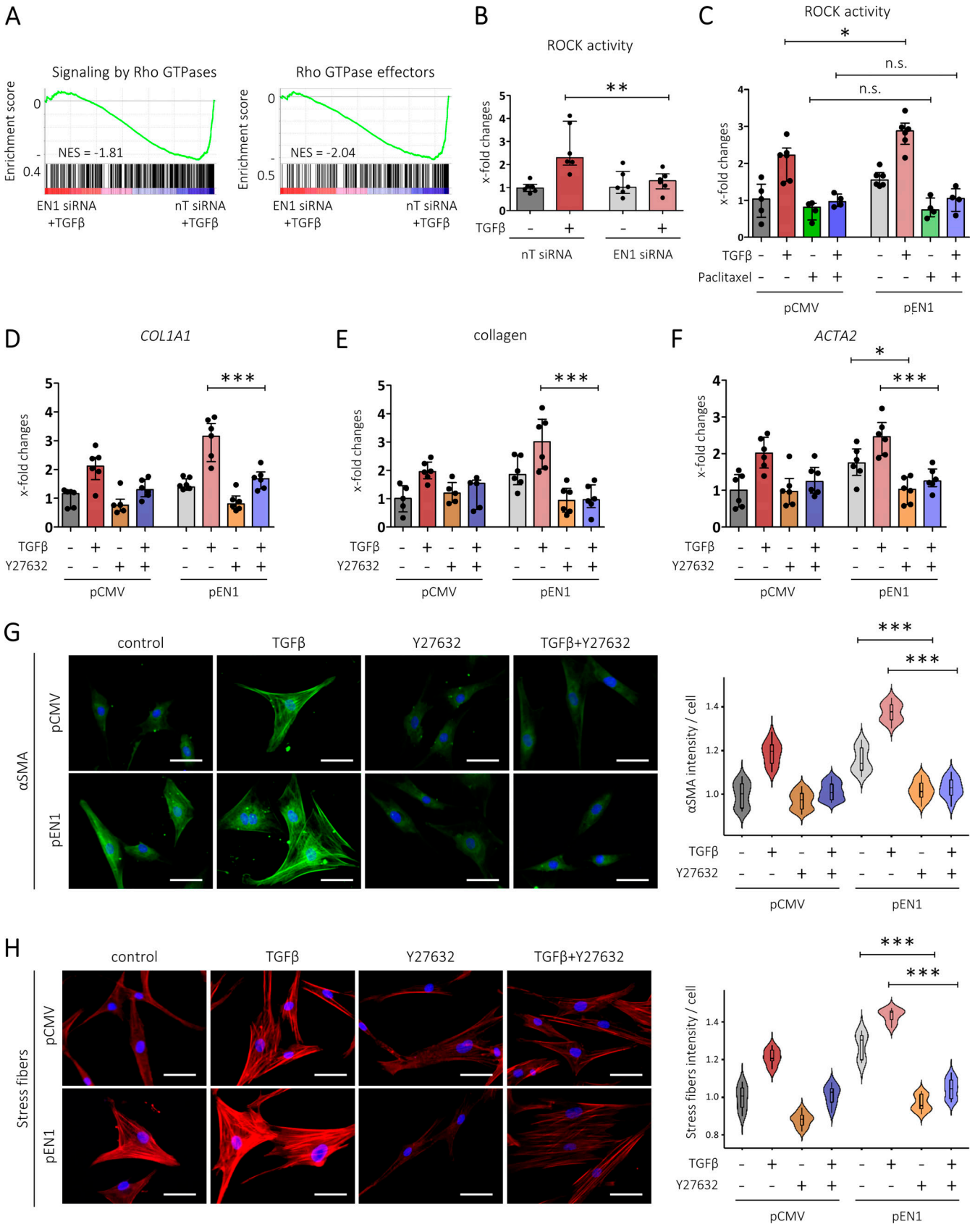

Figure 8. **EN1 induces ROCK activity to coordinate microtubule-actin cytoskeletal rearrangements and myofibroblast differentiation. (A)** GSEA of the indicated Reactome terms, showing that *EN1* knockdown de-enriches genes related to signaling by Rho GTPases and Rho GTPases effectors. **(B and C)** EN1 induces ROCK activity by depolymerizing microtubules. ROCK activity after *EN1* knockdown (B). ROCK activity after *EN1* overexpression with/without

microtubule stabilization (C). Data for B and C were obtained from two independent experiments ($n \geq 4$). **(D–H)** Pharmacological inhibition of ROCK activity prevents EN1-induced myofibroblast differentiation. Relative mRNA levels of *COL1A1* (D). Relative protein levels of secreted collagen type I (E). Relative mRNA levels of *ACTA2* (F). Representative immunofluorescence stainings for αSMA (G) and stress fibers (H) at 400-fold magnification (scale bars = 50 µm). Quantification of average signal intensity for each cell (relative to control) is included. Data for D–H were obtained from two independent experiments ($n \geq 4$). All data are represented as median ± interquartile range. P values are expressed as follows: *, 0.05 > P > 0.01; **, 0.01 > P > 0.001; ***, P < 0.001 (ANOVA with Tukey's post hoc test).

murine fibroblasts isolated from *En1*$^{fl/fl}$ mice, Cre-mediated recombination was induced by infection with type 5 adenoviral vectors encoding for Cre recombinase at a multiplicity of infection of 80 (Palumbo-Zerr et al., 2017). Type 5 adenoviral vectors encoding for LacZ served as controls. In selective experiments, cells were stimulated with recombinant TGFβ (10 ng/ml; PeproTech) for 24 h, unless stated otherwise. In certain experiments, microtubules were stabilized by addition of paclitaxel (1 µM); depolymerized by addition of vinblastine (1 µM); or activity of Rho kinase 1 and 2 was inhibited by Y27632 (1 µM).

3D full-thickness skin equivalents

3D full-thickness skin equivalents were generated with human fibroblasts transfected with 0.5 µg of plasmid encoding for *EN1* or a *CMV* control vector. After transfection, fibroblasts (4×10^5 cells for each replicate) were suspended in neutralization solution (232.5 ml DMEM/F12, 7.5 ml FBS, 7.5 ml 3 M HEPES, and 2.5 ml chondroitin sulfate) and mixed with rat tail collagen type 1 (10 mg/ml). 500 µl of neutralized fibroblast–containing collagen (2 parts of collagen to 1 part neutralization solution containing fibroblasts) was added in each cell-culture insert with porous membranes (8 µm; Greiner Bio One), to create the dermal-like part. The dermal components were cultured for 1 d in DMEM supplemented with 10% FBS, 1% penicillin/streptomycin at 37°C, 5% CO_2, and atmospheric O_2. The epidermal component was generated by seeding 5×10^5 normal human epidermal keratinocytes for each replicate resuspended in Epilife medium with 1% human keratinocyte growth supplement (Gibco BRL) and with extra 1.44 mM $CaCl_2$ on the apical surface of the dermal components on the following day. 1 d later, the full-thickness skin models were cultured in Epilife medium supplemented with 1% human keratinocyte growth supplement (Gibco BRL), 1.44 mM $CaCl_2$, 0.125 mM L-ascorbic acid 2-phosphate, and 10 ng/ml keratinocyte growth factor (Sigma-Aldrich) at an air-liquid interface and treated with paclitaxel (1 µM) or Y27632 (1 µM).

RNA-seq

Total RNA from *EN1*-knockdown and control human fibroblasts stimulated with TGFβ (with three biological replicates per condition) was extracted as described (Wohlfahrt et al., 2019). RNA-seq was performed by Novogene (Cambridge, UK) on an Illumina NovaSeq platform using a paired-end 150-bp sequencing strategy. Read counts were normalized by trimmed mean of M values method for analysis with edgeR and limma-voom. For analysis with DESeq2, the internal normalization method listed on the package was used (Fuchs et al., 2020). Differential gene expression analysis was performed using edgeR, limma-voom, and DESeq2 R packages, with the following thresholds for differential expression: Benjamini–Hochberg adjusted P value/false discovery rate <0.25 and fold-change >1.5. Genes that were identified as differentially expressed by at least two of the three methods were defined as high-confidence DEGs and used for downstream analyses. Heatmaps were generated using pheatmap package. Dot plots were generated with ggplot2 R package. Functional enrichment analysis was performed using the g:Profiler web tool with a threshold of 0.05 for adjusted P values using the GO, Reactome, KEGG, and Wiki Pathways databases (Raudvere et al., 2019). Gene ratios of selected GO or Reactome terms were plotted as dot plots. GSEA was performed using GSEA software v3.0 (Broad Institute) with previously curated gene sets from the Molecular Signatures Database and a threshold of 0.25 for false discovery rate–corrected *q* value (Subramanian et al., 2005). The RNA-seq datasets were deposited in the GEO database (accession no. GSE174598).

In silico analysis of the promoters of DEGs

Flanking regions (−800) of up- and down-regulated DEGs were retrieved from Ensembl database (GRCh38.p13). Negative control sequences of the same length were generated with random ACTG dummy sequences using Perl. Transcription factor profiling analysis against all human matrices extracted from JASPAR2018 database was performed with sequence scanning from TFBStools package v1.26.0 (Tan and Lenhard, 2016) using R version 4.0.0. The top 1% of results sorted by calculated binding scores was used for further analysis. Transcription factor enrichment was calculated by the ratio of genes predicted for one transcription factor relative to the total number of up- and down-regulated genes used in the analysis. Transcription factors with >20% promotor binding were selected as significant. Functional analysis was performed using g:Profiler web tool (Raudvere et al., 2019). Results of the transcription factor analysis are presented in circular packing plots generated with ggraph package v2.0.3 (https://cran.rstudio.com/web/packages/ggraph/).

Quantitative real-time PCR

Total RNA was isolated with the NucleoSpin RNA II extraction system (Macherey-Nagel) and reverse transcribed into cDNA. Gene expression was quantified by real-time PCR using the Mx3005P Sequence Detection System (Agilent Technologies). Primers were designed with Primer3 software and are listed in Table S1. Samples without enzyme in the reverse transcription reaction were used as negative controls. Unspecific signals caused by primer dimers were excluded by nontemplate controls and by dissociation curve analysis. β-Actin was used to normalize for the amounts of cDNA within each sample. Differences were calculated with the threshold cycle (Ct) and the

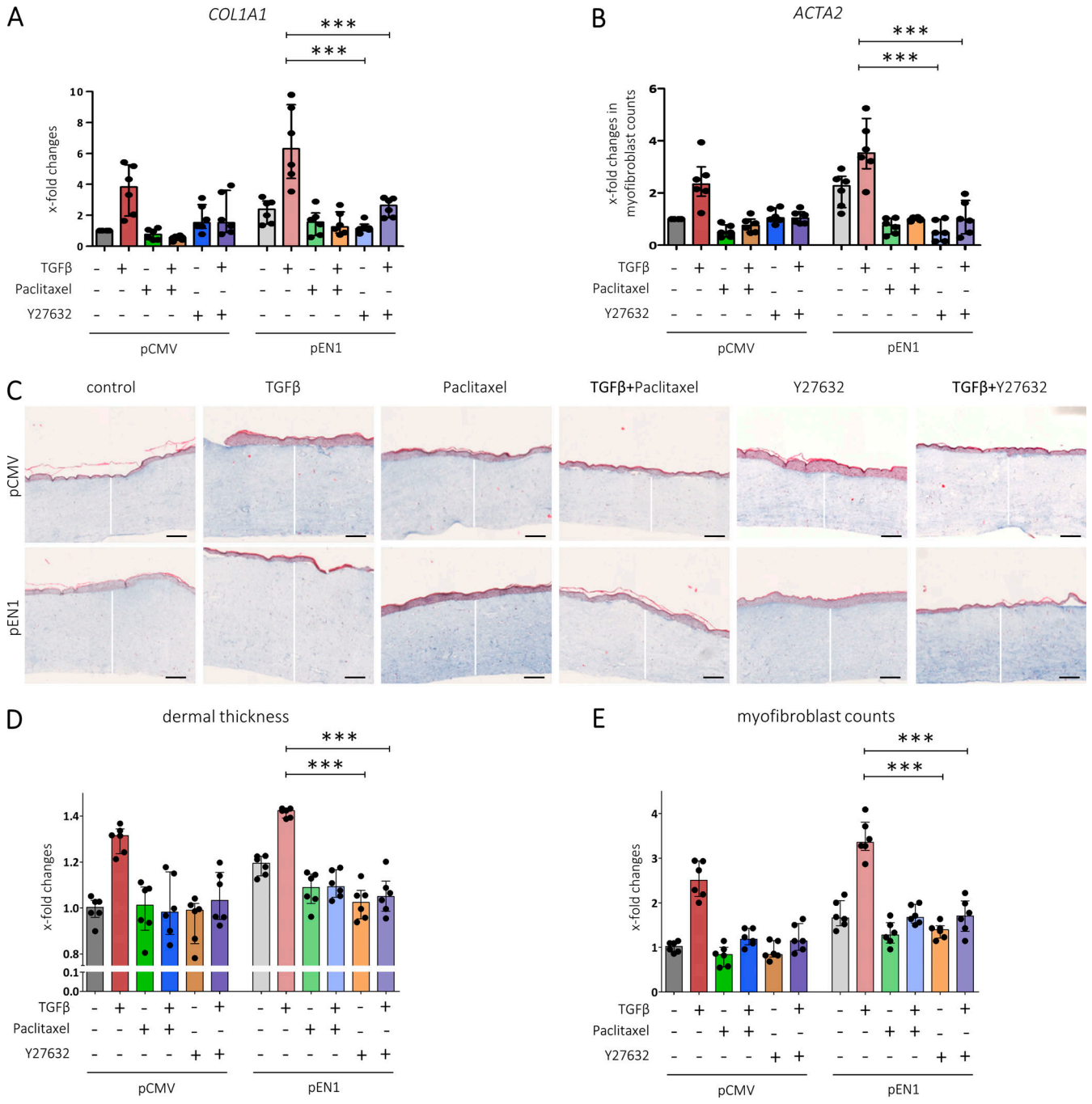

Figure 9. **EN1 promotes TGFβ-induced fibrotic transformation of 3D skin equivalents in a microtubule- and ROCK-dependent manner. (A–E)** Pharmacological stabilization of microtubules or inhibition of ROCK activity prevents EN1-mediated fibrotic transformation of 3D skin equivalents. Relative mRNA levels of *COL1A1* (A) and *ACTA2* (B). Representative trichrome stainings of skin models, acquired with a slide scanner at 40× magnification; adjacent pictures of the same slide were stitched to generate overview pictures; white bars indicate dermal thickness (scale bars = 200 µm; C). Quantification of dermal thickness (D) and of myofibroblast counts (E). All data are represented as median ± interquartile range of $n = 6$ independent biological samples per group from two independent experiments. P values are expressed as follows: ***, $P < 0.001$ (ANOVA with Tukey's post hoc test).

comparative Ct method for relative quantification (Dees et al., 2020).

Western blot analysis

The soluble and insoluble fractions of α-Tubulin were extracted as described (Sandbo et al., 2013). The total protein concentration of cell lysates was determined by Bradford assay (#5000001; Bio-Rad). Proteins were separated by SDS-PAGE and transferred to a polyvinylidene difluoride membrane. The membrane was incubated with primary antibodies against EN1 (1:200; Santa Cruz Biotechnology), β-ACTIN (1:10,000, #A5441; Sigma-Aldrich), p-SMAD3 (1:1,000, #9520; Cell Signaling), αSMA (1:1,000, #A5228; Sigma-Aldrich), α-Tubulin (1:1,000, #14-4502-82; Thermo Fisher Scientific), SP1 (#9389S; Cell Signaling), and HRP-conjugated

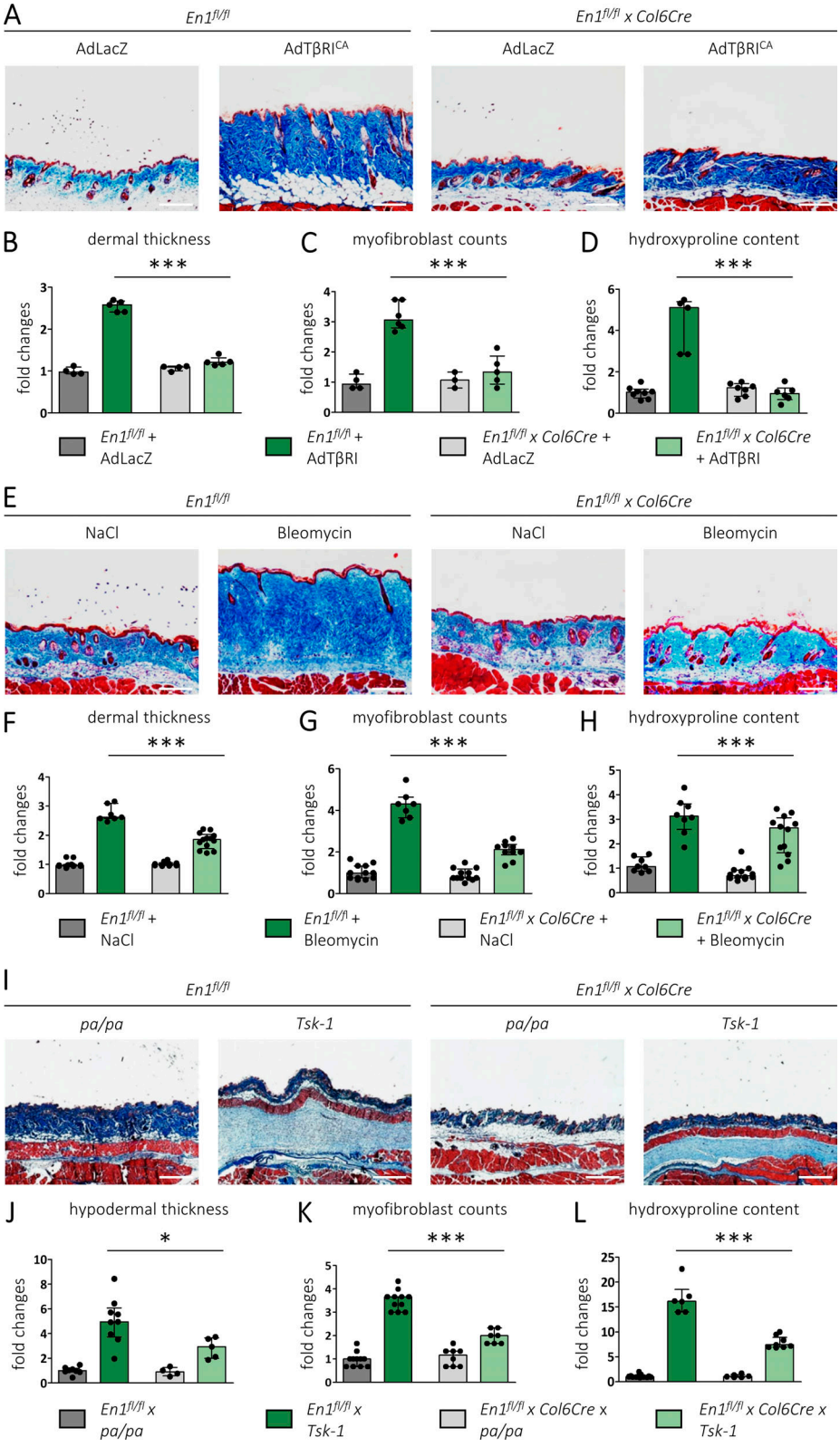

Figure 10. **Fibroblast-specific knockout of *En1* ameliorates experimental skin fibrosis. (A–D)** TBRI^{CA} mice with fibroblast-specific knockout of *En1* are protected from skin fibrosis. Representative trichrome stainings of the skin shown at 100× magnification (scale bars = 200 µm; A). Quantification of dermal thickness (B), myofibroblast counts (C), and hydroxyproline content (D), with figure legend under the plots. **(E–H)** Bleomycin-challenged mice with fibroblast-specific knockout of *En1* are protected from skin fibrosis. Representative trichrome stainings of the skin shown at 100× magnification (scale bars = 200 µm; E). Quantification of dermal thickness (F), myofibroblast counts (G), and hydroxyproline content (H), with figure legend under the plots. **(I–L)** Tsk-1 mice with fibroblast-specific knockout of *En1* are protected from skin fibrosis. Representative trichrome stainings of the skin shown at 40× magnification (I).

Quantification of dermal thickness (J), myofibroblast counts (K), and hydroxyproline content (L), with figure legend under the plots (scale bars = 500 µm). All data for A–L are represented as median ± interquartile range of $n \geq 5$ independent biological samples per group from at least two independent experiments. P values are expressed as follows: *, 0.05 > P > 0.01; ***, P < 0.001 (ANOVA with Tukey's post hoc test).

secondary antibodies (1:5,000; Dako). Blots were visualized by ECL. β-Actin was used as loading control. Western blots were quantified using ImageJ software.

Coimmunoprecipitation

Fibroblasts were collected in lysis buffer, as for Western blot. 10% of the amount of protein used for immunoprecipitation was used as input. Cell extracts were incubated with 30 µl protein A/G Sepharose and 5 µg of either SP1 or rabbit IgG antibody (#9389S; Cell Signaling; and #NI01; Millipore). Unbound proteins were removed by washing with lysis buffer. Sepharose-bound protein complexes were separated via SDS-PAGE followed by Western blotting on a polyvinylidene difluoride membrane (see Western blot analysis).

ChIP PCR and sequencing

ChIP assays, including purification of the enriched DNA, were performed using the ChIP-IT High Sensitivity Kit (Active Motif). In brief, 20–30 µg of sonicated chromatin extract was incubated with 1 µg of antibodies against SMAD3, EN1, or SP1 (SMAD3, #9523S; SP1, #9389S; both Cell Signaling; EN1, NBP2-57757; Novus Biologicals) or rabbit IgG antibody (#NI01; Millipore). SMAD3 binding in EN1 promoter was determined by PCR of the enriched DNA (after immunoprecipitation with an antibody against SMAD3) using the following primer pairs: 5′-TTCTAT GGCCTCTGGACGTG-3′ (forward) and 5′-ACTGTCGCTGAGAGA TTCGT-3′ (reverse) and 5′-CTGAGTGTCAGCGCGAGTT-3′ (forward) and 5′-TTTTGCCTTCAAACCGGAAGC-3′ (reverse).

Enriched DNA after immunoprecipitation with antibodies against EN1 or SP1 from *EN1* knockdown and control human fibroblasts stimulated with TGFβ (with three biological replicates per condition) was sequenced by Novogene on an Illumina NovaSeq 6000 platform. Alignment to the GRCh37 reference genome was performed using Bowtie2 software (Langmead and Salzberg, 2012), and the generated result bam files were sorted with samtools (Li, 2011) and parsed by MACS v2.2.7.1 (Feng et al., 2012) for peak calling. Consequently, the results were assessed by ChIPQC library (Carroll et al., 2014), and peak annotation was performed using ChIPseeker (Yu et al., 2015). The promoter regions were then carefully extracted for pairwise comparison with the differential gene expression results, down- and up-regulated, respectively. Functional enrichment analysis was completed using g:Profiler, and figures were plotted using ggplot2 library. The ChIP-seq datasets were deposited in the GEO database (accession no. GSE174580).

Quantification of collagen protein

The amount of soluble collagen in cell culture supernatants was quantified using the SirCol collagen assay (Biocolor). The total collagen content of skin tissue samples was determined by hydroxyproline assay as described previously (Zehender et al., 2018; Zhang et al., 2017).

ECM staining

ECM staining was performed as described (Chakraborty et al., 2020). An equal number of fibroblasts (3×10^3/well for 384-well plates) was seeded in each well of dark-walled imaging plates (BD Biosciences). After 5 d of incubation with or without stimulation with recombinant TGFβ (10 ng/ml), IL-11 (10 ng/ml), IL-13 (100 ng/ml), or CTGF (50 ng/ml) at 37°C and 5% CO_2, cells were washed in PBS and lysed with 0.25 M ammonium hydroxide in 25 mM Tris for 3 min at 37°C. Before cell lysis, Preston Blue staining was performed to account for differences in cell viability between conditions. The matrix was washed three times in PBS, fixed using 100% methanol for 30 min at −20°C, and then stained with anti-Fibronectin Alexa Fluor 488 (1:200; eBioscience), anti-collagen type I antibody (1:200; Sigma-Aldrich), and anti-collagen type III (1:200, Millipore). The ECM stainings were imaged using the CellInsight CX5 High Content Screening Platform (Thermo Fisher Scientific), and total intensity per well was automatically quantified using a custom pipeline in HCS Studio Cell Analysis software, normalized to cell viability, and represented as a violin plot for each condition using ggplot2.

Immunohistochemistry and immunofluorescence staining

Formalin-fixed, paraffin-embedded skin sections or fibroblasts fixed in 4% paraformaldehyde and permeabilized by 0.25% Triton X-100 were stained as described (Matei et al., 2019). Primary antibodies used were against EN1 (1:50, #83693; Abcam), P4Hβ (1:50, #MA3-019; Thermo Fisher Scientific), vimentin (1:200, #20346; Abcam), CD45 (1:100, #sc-59070; Santa Cruz Biotechnology), CD31 (1:100, #AF3628; R&D Systems), αSMA (1:1,000, #A5228; Sigma-Aldrich), and α-Tubulin (1:500, #T9026; Sigma-Aldrich). Alexa Fluor–conjugated secondary antibodies (Thermo Fisher Scientific) were used (1:200). Isotype-matched antibodies were used as negative controls. Stress fibers were visualized with rhodamine-conjugated phalloidin (1:40, #R415; Sigma-Aldrich). Nuclei were counterstained using DAPI (1:800, #sc-3598; Santa, Cruz Biotechnology). The stains of human or murine skin tissues were analyzed using an Eclipse 80i microscope (Nikon), and quantification of percentages of EN1-positive fibroblasts was performed using a custom CellProfiler 3.0 pipeline (McQuin et al., 2018). Voronoi tessellation of immunofluorescence stainings was performed using Fiji software as described (Matei et al., 2018; Schindelin et al., 2012). The stains of cultured cells were analyzed using the CellInsight CX5 High Content Screening Platform (Thermo Fisher Scientific), and average or total intensity per cell was automatically quantified using a custom pipeline in HCS Studio Cell Analysis software and represented as a violin plot for each condition using ggplot2.

IMC: Staining and data analysis

IMC was performed as described (Giesen et al., 2014). The antibodies were acquired preconjugated (Fluidigm) or in purified

preparations. All the purified antibodies were first validated by standard immunofluorescence staining. Purified antibodies were consequently conjugated to lanthanide metals using the Maxpar X8 antibody labeling kit (Fluidigm) following the manufacturer's instructions. The complete panel was once more validated in IMC, and all the antibodies were titrated in IMC. Paraffin-embedded skin sections (5 µm) were deparaffinized with xylene for 30 min and rehydrated in a graded series of alcohol (ethanol:deionized water 100:0, 100:0, 90:10, and 80:20 for 5 min each). For epitope retrieval, the slides were incubated for 30 min in preheated Tris-EDTA buffer (10 mM Tris base, 1 mM EDTA, and 0.05% Tween 20, pH 9). After slides were cooled, they were blocked with 2% BSA in PBS for 1 h at room temperature. Samples were incubated overnight at 4°C with the metal-labeled antibody mix (in 0.5% BSA). The antibodies are listed in Table S3. Tissue samples were washed once in PBS-T (PBS and 0.2% Tween 20) and twice in PBS for 5 min each. DNA staining was performed with Iridium-Intercalator (125 µM) 1/400 for 5 min at room temperature. Afterward, the samples were washed three times in PBS and once in deionized water for 5 min each. Finally, the tissue sections were dried, stored, and shipped at room temperature.

Imaging was performed using a Hyperion Imaging System (Fluidigm) by the group of Prof. Dr. Bertram Bengsch (Department of Medicine II: Gastroenterology, Hepatology, Endocrinology, and Infectious Disease, University Medical Center Freiburg). The MCD files were converted to TIFF format, segmented into single cells using a publicly available analysis pipeline (https://zenodo.org/record/3841961), and analyzed with histoCAT with logarithmic data normalization (Schapiro et al., 2017) and FlowJo software (BD Life Sciences). Before applying the Phenograph clustering (Levine et al., 2015), all epithelial cells (E-cadherin$^+$) and immune cells (CD45$^+$) were excluded. Finally, t-distributed stochastic neighbor embedding (tSNE) plots were generated using a custom Python script.

ROCK activity assay

The activity of ROCK in lysates of human fibroblasts was measured by ROCK activity assay according to the manufacturer's instructions (#CSA001; Millipore).

Statistics

All data are presented as median ± interquartile range. For a two-group comparison, Mann–Whitney *U* test for nonparametric data was used. When more than two groups of samples were compared, one-way ANOVA with Tukey's range test as post hoc analysis was used. P values <0.05 were considered statistically significant. P values are expressed as follows: *, 0.05 > P > 0.01; **, 0.01 > P > 0.001; and ***, P < 0.001. GraphPad Prism software v8.0 was used for statistical analysis. The sample size was estimated based on previous experiments. No statistical method was used to predetermine sample size.

Online supplemental material

Fig. S1 shows EN1 expression in healthy and SSc skin in endothelial cells, leukocytes and keratinocytes, as well as compositions of IMC clusters and EN1 expression across clusters in dorsal and ventral skin. Fig. S2 shows that knockout of *En1* in murine fibroblasts prevents TGFβ-induced fibroblast activation. Fig. S3 represents the effects of *EN1* overexpression on IL-11–, IL-13–, and CTGF-induced fibroblast activation. Fig. S4 lists the transcription factors with enriched binding motifs in the promoters of EN1-DEGs and the transcription factors with predicted cobinding with EN1-SP-DEGs with enriched motifs only in up- or down-regulated DEGs. Fig. S5 shows that knockdown of *EN1* prevents myofibroblast differentiation by inducing microtubule stabilization. Table S1 lists the primers used for quantitative real-time PCR. Table S2 lists the clinical data of the SSc patients. Table S3 lists the antibodies used in the IMC panel. Table S4 and Table S5 show transcription factor binding site enrichments in the promoters of EN1-DEGs and EN1-SP-DEGs, respectively. Table S6 shows functional enrichment analysis of the EN1-SP-DEGs.

Data availability

All data generated or analyzed during this study are included in this published article (and supplemental files). Additional supporting information are available from the corresponding author on reasonable request.

Acknowledgments

We thank Wolfgang Espach, Lena Summa, Christoph Liebel, Regina Kleinlein, Katja Dreißigacker, and Vladyslav Fedorchenko for excellent technical assistance.

This work was supported by the German Research Foundation (grants DI 1537/9-1, DI 1537/9-2, DI 1537/11-1, DI 1537/12-1, DI 1537/13-1, DI 1537/14-1, DI 1537/17-1, MA 9219/2-1, BE 7306/2-1, DE 2414/2-1, and DE 2414/4-1; INST 90/1095-1 FUGG, SFB CRC1181 [project C01], and SFB TR221 project number 324392634 [B04]), the Interdisciplinary Center for Clinical Research in Erlangen (grants J39 and A79), the Else Kröner-Fresenius Foundation (grants 2021_EKEA.03, 2014_A47, and 2014_A248), the ELAN-Foundation Erlangen (grants 14-12-17-1-Bergmann and 19-12-06-1-Matei), the German Ministry of Education and Research (Era-Net grant 01KT1801 and CompLS grant 031L0262C), and a Career Support Award of Medicine of the Ernst Jung Foundation.

Author contributions: A.-H. Györfi, A.-E. Matei, and J.H.W. Distler designed the study. A.-H. Györfi, A.-E. Matei, M. Fuchs, A.R.-R., C. Liang, X. Hong, H Zhu., M. Luber, C. Bergmann, C. Dees, and M. Kunz were involved in acquisition of data. A.-H. Györfi, A.-E. Matei, M. Fuchs, A. Rius Rigau, C. Liang, H. Zhu, O. Distler, J. Wang, B. Bengsch, G. Schett, M. Kunz, and J.H.W. Distler were involved in interpretation of data. I. Ludolph and R.E. Horch provided essential samples. A.-H. Györfi, A.-E. Matei, M. Kunz, and J.H.W. Distler wrote the manuscript with feedback from all authors.

Disclosures: C. Bergmann reported personal fees from Boehringer Ingelheim and Pfizer during the conduct of the study. O. Distler reported personal fees from Abbvie, Acceleron Pharma, Amgen, AnaMar, Arxx Therapeutics, Baecon Discovery, Blade Therapeutics, Bayer, Böhringer Ingelheim, ChemomAb, Corbus

Pharmacheuticals, CSL Behring, Galapagos NV, Glenmark Pharmaceuticals, GSK, Horizon Pharmaceuticals, Inventiva, Iqvia, Italfarmaco, Iqone, Kymera Therapeutics, Lupin Pharmaceuticals, Medac, Medscape, Mitsubishi Tanabe Pharma, MSD, Novartis, Pfizer, Roche, Roivant, Sanofi, Serodapharm, Topadur, Target Bioscience, and UCB during the conduct of the study; in addition, O. Distler had a patent to mir-29 for the treatment of systemic sclerosis issued (US8247389, EP2331143). J.H.W. Distler reported personal fees from Janssen, Anamar, ARXX, Bayer Pharma, Boehringer Ingelheim, Galapagos, GSK, Inventiva, Novartis, and UCB; grants from Anamar, ARXX, aTyr, Bayer Pharma, Boehringer Ingelheim, Cantargia, Celgene, CSL Behring, Galapagos, Inventiva, Kiniksa, and UCB outside the submitted work; and owns stock in 4D Science. No other disclosures were reported.

Submitted: 3 September 2020
Revised: 5 April 2021
Accepted: 24 May 2021

References

Aguilar-Hidalgo, D., M.A. Domínguez-Cejudo, G. Amore, A. Brockmann, M.C. Lemos, A. Córdoba, and F. Casares. 2013. A Hh-driven gene network controls specification, pattern and size of the Drosophila simple eyes. *Development.* 140:82–92. https://doi.org/10.1242/dev.082172

Akhmetshina, A., K. Palumbo, C. Dees, C. Bergmann, P. Venalis, P. Zerr, A. Horn, T. Kireva, C. Beyer, J. Zwerina, et al. 2012. Activation of canonical Wnt signalling is required for TGF-β-mediated fibrosis. *Nat. Commun.* 3: 735. https://doi.org/10.1038/ncomms1734

Alexandre, C., and J.P. Vincent. 2003. Requirements for transcriptional repression and activation by Engrailed in Drosophila embryos. *Development.* 130:729–739. https://doi.org/10.1242/dev.00286

Armaka, M., M. Apostolaki, P. Jacques, D.L. Kontoyiannis, D. Elewaut, and G. Kollias. 2008. Mesenchymal cell targeting by TNF as a common pathogenic principle in chronic inflammatory joint and intestinal diseases. *J. Exp. Med.* 205:331–337. https://doi.org/10.1084/jem.20070906

Beltran, A.S., L.M. Graves, and P. Blancafort. 2014. Novel role of Engrailed 1 as a prosurvival transcription factor in basal-like breast cancer and engineering of interference peptides block its oncogenic function. *Oncogene.* 33:4767–4777. https://doi.org/10.1038/onc.2013.422

Bergmann, C., and J.H. Distler. 2016. Canonical Wnt signaling in systemic sclerosis. *Lab. Invest.* 96:151–155. https://doi.org/10.1038/labinvest.2015.154

Bershadsky, A., A. Chausovsky, E. Becker, A. Lyubimova, and B. Geiger. 1996. Involvement of microtubules in the control of adhesion-dependent signal transduction. *Curr. Biol.* 6:1279–1289. https://doi.org/10.1016/S0960-9822(02)70714-8

Beyer, C., and J.H. Distler. 2013. Morphogen pathways in systemic sclerosis. *Curr. Rheumatol. Rep.* 15:299. https://doi.org/10.1007/s11926-012-0299-6

Beyer, C., N. Reich, S.C. Schindler, A. Akhmetshina, C. Dees, M. Tomcik, C. Hirth-Dietrich, G. von Degenfeld, P. Sandner, O. Distler, et al. 2012a. Stimulation of soluble guanylate cyclase reduces experimental dermal fibrosis. *Ann. Rheum. Dis.* 71:1019–1026. https://doi.org/10.1136/annrheumdis-2011-200862

Beyer, C., G. Schett, S. Gay, O. Distler, and J.H. Distler. 2009. Hypoxia. Hypoxia in the pathogenesis of systemic sclerosis. *Arthritis Res. Ther.* 11: 220. https://doi.org/10.1186/ar2598

Beyer, C., G. Schett, O. Distler, and J.H. Distler. 2010. Animal models of systemic sclerosis: prospects and limitations. *Arthritis Rheum.* 62: 2831–2844. https://doi.org/10.1002/art.27647

Beyer, C., A. Schramm, A. Akhmetshina, C. Dees, T. Kireva, K. Gelse, S. Sonnylal, B. de Crombrugghe, M.M. Taketo, O. Distler, et al. 2012b. β-catenin is a central mediator of pro-fibrotic Wnt signaling in systemic sclerosis. *Ann. Rheum. Dis.* 71:761–767. https://doi.org/10.1136/annrheumdis-2011-200568

Carroll, T.S., Z. Liang, R. Salama, R. Stark, and I. de Santiago. 2014. Impact of artifact removal on ChIP quality metrics in ChIP-seq and ChIP-exo data. *Front. Genet.* 5:75. https://doi.org/10.3389/fgene.2014.00075

Chakraborty, D., B. Šumová, T. Mallano, C.W. Chen, A. Distler, C. Bergmann, I. Ludolph, R.E. Horch, K. Gelse, A. Ramming, et al. 2017. Activation of STAT3 integrates common profibrotic pathways to promote fibroblast activation and tissue fibrosis. *Nat. Commun.* 8:1130. https://doi.org/10.1038/s41467-017-01236-6

Chakraborty, D., H. Zhu, A. Jüngel, L. Summa, Y.N. Li, A.E. Matei, X. Zhou, J. Huang, T. Trinh-Minh, C.W. Chen, et al. 2020. Fibroblast growth factor receptor 3 activates a network of profibrotic signaling pathways to promote fibrosis in systemic sclerosis. *Sci. Transl. Med.* 12:eaaz5506. https://doi.org/10.1126/scitranslmed.aaz5506

Chang, Y.C., P. Nalbant, J. Birkenfeld, Z.F. Chang, and G.M. Bokoch. 2008. GEF-H1 couples nocodazole-induced microtubule disassembly to cell contractility via RhoA. *Mol. Biol. Cell.* 19:2147–2153. https://doi.org/10.1091/mbc.e07-12-1269

Córdova, G., A. Rochard, C. Riquelme-Guzmán, C. Cofré, D. Scherman, P. Bigey, and E. Brandan. 2015. SMAD3 and SP1/SP3 Transcription Factors Collaborate to Regulate Connective Tissue Growth Factor Gene Expression in Myoblasts in Response to Transforming Growth Factor β. *J. Cell. Biochem.* 116:1880–1887. https://doi.org/10.1002/jcb.25143

Danielian, P.S., and A.P. McMahon. 1996. Engrailed-1 as a target of the Wnt-1 signalling pathway in vertebrate midbrain development. *Nature.* 383: 332–334. https://doi.org/10.1038/383332a0

Dees, C., C. Beyer, A. Distler, A. Soare, Y. Zhang, K. Palumbo-Zerr, O. Distler, G. Schett, P. Sandner, and J.H. Distler. 2015. Stimulators of soluble guanylate cyclase (sGC) inhibit experimental skin fibrosis of different aetiologies. *Ann. Rheum. Dis.* 74:1621–1625. https://doi.org/10.1136/annrheumdis-2014-206809

Dees, C., S. Pötter, Y. Zhang, C. Bergmann, X. Zhou, M. Luber, T. Wohlfahrt, E. Karouzakis, A. Ramming, K. Gelse, et al. 2020. TGF-β-induced epigenetic deregulation of SOCS3 facilitates STAT3 signaling to promote fibrosis. *J. Clin. Invest.* 130:2347–2363. https://doi.org/10.1172/JCI122462

Dees, C., M. Tomcik, P. Zerr, A. Akhmetshina, A. Horn, K. Palumbo, C. Beyer, J. Zwerina, O. Distler, G. Schett, and J.H. Distler. 2011a. Notch signalling regulates fibroblast activation and collagen release in systemic sclerosis. *Ann. Rheum. Dis.* 70:1304–1310. https://doi.org/10.1136/ard.2010.134742

Dees, C., P. Zerr, M. Tomcik, C. Beyer, A. Horn, A. Akhmetshina, K. Palumbo, N. Reich, J. Zwerina, M. Sticherling, et al. 2011b. Inhibition of Notch signaling prevents experimental fibrosis and induces regression of established fibrosis. *Arthritis Rheum.* 63:1396–1404. https://doi.org/10.1002/art.30254

Distler, J.H., C. Feghali-Bostwick, A. Soare, Y. Asano, O. Distler, and D.J. Abraham. 2017. Review: Frontiers of Antifibrotic Therapy in Systemic Sclerosis. *Arthritis Rheumatol.* 69:257–267. https://doi.org/10.1002/art.39865

Distler, J.H.W., A.H. Györfi, M. Ramanujam, M.L. Whitfield, M. Königshoff, and R. Lafyatis. 2019. Shared and distinct mechanisms of fibrosis. *Nat. Rev. Rheumatol.* 15:705–730. https://doi.org/10.1038/s41584-019-0322-7

Dugina, V., L. Fontao, C. Chaponnier, J. Vasiliev, and G. Gabbiani. 2001. Focal adhesion features during myofibroblastic differentiation are controlled by intracellular and extracellular factors. *J. Cell Sci.* 114:3285–3296. https://doi.org/10.1242/jcs.114.18.3285

Feng, J., T. Liu, B. Qin, Y. Zhang, and X.S. Liu. 2012. Identifying ChIP-seq enrichment using MACS. *Nat. Protoc.* 7:1728–1740. https://doi.org/10.1038/nprot.2012.101

Fuchs, M., F.P. Kreutzer, L.A. Kapsner, S. Mitzka, A. Just, F. Perbellini, C.M. Terracciano, K. Xiao, R. Geffers, C. Bogdan, et al. 2020. Integrative Bioinformatic Analyses of Global Transcriptome Data Decipher Novel Molecular Insights into Cardiac Anti-Fibrotic Therapies. *Int. J. Mol. Sci.* 21:4727. https://doi.org/10.3390/ijms21134727

Gabrielli, A., E.V. Avvedimento, and T. Krieg. 2009. Scleroderma. *N. Engl. J. Med.* 360:1989–2003. https://doi.org/10.1056/NEJMra0806188

Gandhi, N.S., P. Blancafort, and R.L. Mancera. 2018. Atomistic molecular dynamics simulations of bioactive engrailed 1 interference peptides (EN1-iPeps). *Oncotarget.* 9:22383–22397. https://doi.org/10.18632/oncotarget.25025

Giesen, C., H.A. Wang, D. Schapiro, N. Zivanovic, A. Jacobs, B. Hattendorf, P.J. Schüffler, D. Grolimund, J.M. Buhmann, S. Brandt, et al. 2014. Highly multiplexed imaging of tumor tissues with subcellular resolution by mass cytometry. *Nat. Methods.* 11:417–422. https://doi.org/10.1038/nmeth.2869

Györfi, A.H., A.E. Matei, and J.H.W. Distler. 2018. Targeting TGF-β signaling for the treatment of fibrosis. *Matrix Biol.* 68-69:8–27. https://doi.org/10.1016/j.matbio.2017.12.016

Hanks, M., W. Wurst, L. Anson-Cartwright, A.B. Auerbach, and A.L. Joyner. 1995. Rescue of the En-1 mutant phenotype by replacement of En-1 with En-2. *Science.* 269:679–682. https://doi.org/10.1126/science.7624797

Hinz, B., V. Dugina, C. Ballestrem, B. Wehrle-Haller, and C. Chaponnier. 2003. Alpha-smooth muscle actin is crucial for focal adhesion maturation in myofibroblasts. *Mol. Biol. Cell.* 14:2508–2519. https://doi.org/10.1091/mbc.e02-11-0729

Hinz, B., S.H. Phan, V.J. Thannickal, M. Prunotto, A. Desmoulière, J. Varga, O. De Wever, M. Mareel, and G. Gabbiani. 2012. Recent developments in myofibroblast biology: paradigms for connective tissue remodeling. *Am. J. Pathol.* 180:1340–1355. https://doi.org/10.1016/j.ajpath.2012.02.004

Horikawa, S., Y. Ishii, T. Hamashima, S. Yamamoto, H. Mori, T. Fujimori, J. Shen, R. Inoue, H. Nishizono, H. Itoh, et al. 2015. PDGFRα plays a crucial role in connective tissue remodeling. *Sci. Rep.* 5:17948. https://doi.org/10.1038/srep17948

Jiang, D., D. Correa-Gallegos, S. Christ, A. Stefanska, J. Liu, P. Ramesh, V. Rajendran, M.M. De Santis, D.E. Wagner, and Y. Rinkevich. 2018. Two succeeding fibroblastic lineages drive dermal development and the transition from regeneration to scarring. *Nat. Cell Biol.* 20:422–431. https://doi.org/10.1038/s41556-018-0073-8

Jiang, L., Y. Zhou, M. Xiong, L. Fang, P. Wen, H. Cao, J. Yang, C. Dai, and W. He. 2013. Sp1 mediates microRNA-29c-regulated type I collagen production in renal tubular epithelial cells. *Exp. Cell Res.* 319:2254–2265. https://doi.org/10.1016/j.yexcr.2013.06.007

Kim, Y.J., M. Sung, E. Oh, M.V. Vrancken, J.Y. Song, K. Jung, and Y.L. Choi. 2018. Engrailed 1 overexpression as a potential prognostic marker in quintuple-negative breast cancer. *Cancer Biol. Ther.* 19:335–345. https://doi.org/10.1080/15384047.2018.1423913

Königshoff, M., M. Kramer, N. Balsara, J. Wilhelm, O.V. Amarie, A. Jahn, F. Rose, L. Fink, W. Seeger, L. Schaefer, et al. 2009. WNT1-inducible signaling protein-1 mediates pulmonary fibrosis in mice and is upregulated in humans with idiopathic pulmonary fibrosis. *J. Clin. Invest.* 119:772–787. https://doi.org/10.1172/JCI33950

Krendel, M., F.T. Zenke, and G.M. Bokoch. 2002. Nucleotide exchange factor GEF-H1 mediates cross-talk between microtubules and the actin cytoskeleton. *Nat. Cell Biol.* 4:294–301. https://doi.org/10.1038/ncb773

Lafyatis, R. 2014. Transforming growth factor β--at the centre of systemic sclerosis. *Nat. Rev. Rheumatol.* 10:706–719. https://doi.org/10.1038/nrrheum.2014.137

Langmead, B., and S.L. Salzberg. 2012. Fast gapped-read alignment with Bowtie 2. *Nat. Methods.* 9:357–359. https://doi.org/10.1038/nmeth.1923

Levine, J.H., E.F. Simonds, S.C. Bendall, K.L. Davis, A.D. Amir, M.D. Tadmor, O. Litvin, H.G. Fienberg, A. Jager, E.R. Zunder, et al. 2015. Data-Driven Phenotypic Dissection of AML Reveals Progenitor-like Cells that Correlate with Prognosis. *Cell.* 162:184–197. https://doi.org/10.1016/j.cell.2015.05.047

Li, H. 2011. A statistical framework for SNP calling, mutation discovery, association mapping and population genetical parameter estimation from sequencing data. *Bioinformatics.* 27:2987–2993. https://doi.org/10.1093/bioinformatics/btr509

Liu, B.P., M. Chrzanowska-Wodnicka, and K. Burridge. 1998. Microtubule depolymerization induces stress fibers, focal adhesions, and DNA synthesis via the GTP-binding protein Rho. *Cell Adhes. Commun.* 5:249–255. https://doi.org/10.3109/15419069809040295

Loomis, C.A., E. Harris, J. Michaud, W. Wurst, M. Hanks, and A.L. Joyner. 1996. The mouse Engrailed-1 gene and ventral limb patterning. *Nature.* 382:360–363. https://doi.org/10.1038/382360a0

Manabe, I., T. Shindo, and R. Nagai. 2002. Gene expression in fibroblasts and fibrosis: involvement in cardiac hypertrophy. *Circ. Res.* 91:1103–1113. https://doi.org/10.1161/01.RES.0000046452.67724.B8

Margadant, C., and A. Sonnenberg. 2010. Integrin-TGF-beta crosstalk in fibrosis, cancer and wound healing. *EMBO Rep.* 11:97–105. https://doi.org/10.1038/embor.2009.276

Matei, A.E., C. Beyer, A.H. Györfi, A. Soare, C.W. Chen, C. Dees, C. Bergmann, A. Ramming, A. Friebe, F. Hofmann, et al. 2018. Protein kinases G are essential downstream mediators of the antifibrotic effects of sGC stimulators. *Ann. Rheum. Dis.* 77:459. https://doi.org/10.1136/annrheumdis-2017-212489

Matei, A.E., C.W. Chen, L. Kiesewetter, A.H. Györfi, Y.N. Li, T. Trinh-Minh, X. Xu, C. Tran Manh, T. van Kuppevelt, J. Hansmann, et al. 2019. Vascularised human skin equivalents as a novel in vitro model of skin fibrosis and platform for testing of antifibrotic drugs. *Ann. Rheum. Dis.* 78:1686–1692. https://doi.org/10.1136/annrheumdis-2019-216108

McQuin, C., A. Goodman, V. Chernyshev, L. Kamentsky, B.A. Cimini, K.W. Karhohs, M. Doan, L. Ding, S.M. Rafelski, D. Thirstrup, et al. 2018. CellProfiler 3.0: Next-generation image processing for biology. *PLoS Biol.* 16:e2005970. https://doi.org/10.1371/journal.pbio.2005970

Miura, K., T. Akashi, N. Ando, S. Ayabe, K. Kayamori, T. Namiki, and Y. Eishi. 2018. Homeobox transcriptional factor engrailed homeobox 1 is expressed specifically in normal and neoplastic sweat gland cells. *Histopathology.* 72:1199–1208. https://doi.org/10.1111/his.13486

Ng, B., J. Dong, G. D'Agostino, S. Viswanathan, A.A. Widjaja, W.W. Lim, N.S.J. Ko, J. Tan, S.P. Chothani, B. Huang, et al. 2019. Interleukin-11 is a therapeutic target in idiopathic pulmonary fibrosis. *Sci. Transl. Med.* 11:eaaw1237. https://doi.org/10.1126/scitranslmed.aaw1237

Ng, D.H., J.D. Humphries, A. Byron, A. Millon-Frémillon, and M.J. Humphries. 2014. Microtubule-dependent modulation of adhesion complex composition. *PLoS One.* 9:e115213. https://doi.org/10.1371/journal.pone.0115213

Palumbo-Zerr, K., A. Soare, P. Zerr, A. Liebl, R. Mancuso, M. Tomcik, B. Sumova, C. Dees, C.W. Chen, T. Wohlfahrt, et al. 2017. Composition of TWIST1 dimers regulates fibroblast activation and tissue fibrosis. *Ann. Rheum. Dis.* 76:244–251. https://doi.org/10.1136/annrheumdis-2015-208470

Palumbo-Zerr, K., P. Zerr, A. Distler, J. Fliehr, R. Mancuso, J. Huang, D. Mielenz, M. Tomcik, B.G. Fürnrohr, C. Scholtysek, et al. 2015. Orphan nuclear receptor NR4A1 regulates transforming growth factor-β signaling and fibrosis. *Nat. Med.* 21:150–158. https://doi.org/10.1038/nm.3777

Peluffo, G., A. Subedee, N.W. Harper, N. Kingston, B. Jovanović, F. Flores, L.E. Stevens, F. Beca, A. Trinh, C.S.R. Chilamakuri, et al. 2019. *EN1* Is a Transcriptional Dependency in Triple-Negative Breast Cancer Associated with Brain Metastasis. *Cancer Res.* 79:4173–4183. https://doi.org/10.1158/0008-5472.CAN-18-3264

Raudvere, U., L. Kolberg, I. Kuzmin, T. Arak, P. Adler, H. Peterson, and J. Vilo. 2019. g:Profiler: a web server for functional enrichment analysis and conversions of gene lists (2019 update). *Nucleic Acids Res.* 47(W1):W191–W198. https://doi.org/10.1093/nar/gkz369

Rekaik, H., F.X. Blaudin de Thé, J. Fuchs, O. Massiani-Beaudoin, A. Prochiantz, and R.L. Joshi. 2015. Engrailed Homeoprotein Protects Mesencephalic Dopaminergic Neurons from Oxidative Stress. *Cell Rep.* 13:242–250. https://doi.org/10.1016/j.celrep.2015.08.076

Rinkevich, Y., G.G. Walmsley, M.S. Hu, Z.N. Maan, A.M. Newman, M. Drukker, M. Januszyk, G.W. Krampitz, G.C. Gurtner, H.P. Lorenz, et al. 2015. Skin fibrosis. Identification and isolation of a dermal lineage with intrinsic fibrogenic potential. *Science.* 348:aaa2151. https://doi.org/10.1126/science.aaa2151

Sandbo, N., C. Ngam, E. Torr, S. Kregel, J. Kach, and N. Dulin. 2013. Control of myofibroblast differentiation by microtubule dynamics through a regulated localization of mDia2. *J. Biol. Chem.* 288:15466–15473. https://doi.org/10.1074/jbc.M113.464461

Schafer, S., S. Viswanathan, A.A. Widjaja, W.W. Lim, A. Moreno-Moral, D.M. DeLaughter, B. Ng, G. Patone, K. Chow, E. Khin, et al. 2017. IL-11 is a crucial determinant of cardiovascular fibrosis. *Nature.* 552:110–115. https://doi.org/10.1038/nature24676

Schapiro, D., H.W. Jackson, S. Raghuraman, J.R. Fischer, V.R.T. Zanotelli, D. Schulz, C. Giesen, R. Catena, Z. Varga, and B. Bodenmiller. 2017. histoCAT: analysis of cell phenotypes and interactions in multiplex image cytometry data. *Nat. Methods.* 14:873–876. https://doi.org/10.1038/nmeth.4391

Schindelin, J., I. Arganda-Carreras, E. Frise, V. Kaynig, M. Longair, T. Pietzsch, S. Preibisch, C. Rueden, S. Saalfeld, B. Schmid, et al. 2012. Fiji: an open-source platform for biological-image analysis. *Nat. Methods.* 9:676–682. https://doi.org/10.1038/nmeth.2019

Sgaier, S.K., Z. Lao, M.P. Villanueva, F. Berenshteyn, D. Stephen, R.K. Turnbull, and A.L. Joyner. 2007. Genetic subdivision of the tectum and cerebellum into functionally related regions based on differential sensitivity to engrailed proteins. *Development.* 134:2325–2335. https://doi.org/10.1242/dev.000620

Siracusa, L.D., R. McGrath, Q. Ma, J.J. Moskow, J. Manne, P.J. Christner, A.M. Buchberg, and S.A. Jimenez. 1996. A tandem duplication within the fibrillin 1 gene is associated with the mouse tight skin mutation. *Genome Res.* 6:300–313. https://doi.org/10.1101/gr.6.4.300

Soare, A., A. Ramming, J. Avouac, and J.H. Distler. 2016. Updates on animal models of systemic sclerosis. *J. Scleroderma Relat. Disord.* 1:266–276. https://doi.org/10.5301/jsrd.5000220

Sorolla, A., E. Wang, T.D. Clemons, C.W. Evans, J.H. Plani-Lam, E. Golden, B. Dessauvagie, A.D. Redfern, K. Swaminathan-Iyer, and P. Blancafort. 2019. Triple-hit therapeutic approach for triple negative breast cancers using docetaxel nanoparticles, EN1-iPeps and RGD peptides. *Nanomedicine (Lond.).* 20:102003. https://doi.org/10.1016/j.nano.2019.04.006

Subramanian, A., P. Tamayo, V.K. Mootha, S. Mukherjee, B.L. Ebert, M.A. Gillette, A. Paulovich, S.L. Pomeroy, T.R. Golub, E.S. Lander, and J.P.

Mesirov. 2005. Gene set enrichment analysis: a knowledge-based approach for interpreting genome-wide expression profiles. *Proc. Natl. Acad. Sci. USA.* 102:15545–15550. https://doi.org/10.1073/pnas.0506580102

Sum, C.S., D. Nickischer, M. Lei, A. Weston, L. Zhang, and L. Schweizer. 2014. Establishing a High-content Analysis Method for Tubulin Polymerization to Evaluate Both the Stabilizing and Destabilizing Activities of Compounds. *Curr. Chem. Genomics Transl. Med.* 8(Suppl 1):16–26. https://doi.org/10.2174/2213988501408010016

Sysa, P., J.J. Potter, X. Liu, and E. Mezey. 2009. Transforming growth factor-beta1 up-regulation of human alpha(1)(I) collagen is mediated by Sp1 and Smad2 transacting factors. *DNA Cell Biol.* 28:425–434. https://doi.org/10.1089/dna.2009.0884

Tan, G., and B. Lenhard. 2016. TFBSTools: an R/bioconductor package for transcription factor binding site analysis. *Bioinformatics.* 32:1555–1556. https://doi.org/10.1093/bioinformatics/btw024

van den Hoogen, F., D. Khanna, J. Fransen, S.R. Johnson, M. Baron, A. Tyndall, M. Matucci-Cerinic, R.P. Naden, T.A. Medsger Jr., P.E. Carreira, et al. 2013. 2013 classification criteria for systemic sclerosis: an American college of rheumatology/European league against rheumatism collaborative initiative. *Ann. Rheum. Dis.* 72:1747–1755. https://doi.org/10.1136/annrheumdis-2013-204424

Verrecchia, F., J. Rossert, and A. Mauviel. 2001. Blocking sp1 transcription factor broadly inhibits extracellular matrix gene expression in vitro and in vivo: implications for the treatment of tissue fibrosis. *J. Invest. Dermatol.* 116:755–763. https://doi.org/10.1046/j.1523-1747.2001.01326.x

Villanueva, S., C. Cespedes, A. Gonzalez, and C.P. Vio. 2006. bFGF induces an earlier expression of nephrogenic proteins after ischemic acute renal failure. *Am. J. Physiol. Regul. Integr. Comp. Physiol.* 291:R1677–R1687. https://doi.org/10.1152/ajpregu.00023.2006

Wohlfahrt, T., S. Rauber, S. Uebe, M. Luber, A. Soare, A. Ekici, S. Weber, A.E. Matei, C.W. Chen, C. Maier, et al. 2019. PU.1 controls fibroblast polarization and tissue fibrosis. *Nature.* 566:344–349. https://doi.org/10.1038/s41586-019-0896-x

Wurst, W., A.B. Auerbach, and A.L. Joyner. 1994. Multiple developmental defects in Engrailed-1 mutant mice: an early mid-hindbrain deletion and patterning defects in forelimbs and sternum. *Development.* 120:2065–2075. https://doi.org/10.1242/dev.120.7.2065

Wynn, T.A. 2008. Cellular and molecular mechanisms of fibrosis. *J. Pathol.* 214:199–210. https://doi.org/10.1002/path.2277

Wynn, T.A., and T.R. Ramalingam. 2012. Mechanisms of fibrosis: therapeutic translation for fibrotic disease. *Nat. Med.* 18:1028–1040. https://doi.org/10.1038/nm.2807

Yu, G., L.G. Wang, and Q.Y. He. 2015. ChIPseeker: an R/Bioconductor package for ChIP peak annotation, comparison and visualization. *Bioinformatics.* 31:2382–2383. https://doi.org/10.1093/bioinformatics/btv145

Zehender, A., J. Huang, A.H. Györfi, A.E. Matei, T. Trinh-Minh, X. Xu, Y.N. Li, C.W. Chen, J. Lin, C. Dees, et al. 2018. The tyrosine phosphatase SHP2 controls TGFβ-induced STAT3 signaling to regulate fibroblast activation and fibrosis. *Nat. Commun.* 9:3259. https://doi.org/10.1038/s41467-018-05768-3

Zhang, Y., R. Liang, C.W. Chen, T. Mallano, C. Dees, A. Distler, A. Reich, C. Bergmann, A. Ramming, K. Gelse, et al. 2017. JAK1-dependent transphosphorylation of JAK2 limits the antifibrotic effects of selective JAK2 inhibitors on long-term treatment. *Ann. Rheum. Dis.* 76:1467–1475. https://doi.org/10.1136/annrheumdis-2016-210911

Supplemental material

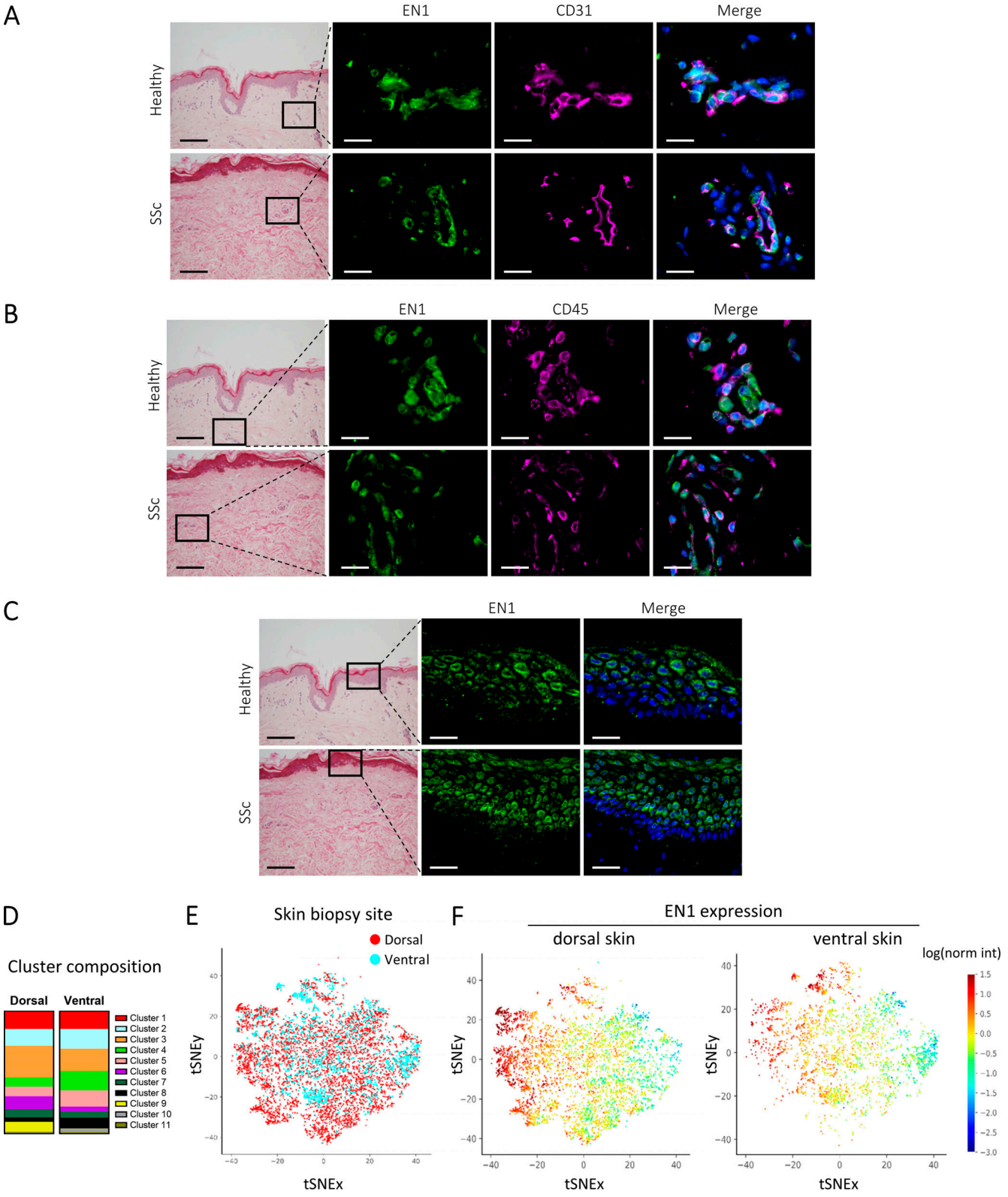

Figure S1. **EN1 expression in healthy and SSc skin. (A–C)** Representative immunofluorescence stainings for EN1 (green) and costainings with CD31 (A) and CD45 (B; both magenta) in the dermis of healthy donors and SSc patients at 1,000-fold magnification (scale bars = 20 µm). Hematoxylin and eosin stainings (200-fold magnification, scale bars = 100 µm) are included. Data for A–C were obtained from $n \geq 4$ biological samples from two independent experiments. **(D)** Composition of clusters from the segmented IMC images in ventral and dorsal skin biopsies from SSc patients. **(E)** tSNE plot showing distribution of cells from ventral and dorsal SSc skin across clusters. **(F)** tSNE plot showing expression of EN1 across the ventral and dorsal SSc clusters. Data for D–F were obtained from $n = 8$ biological samples from four SSc patients (paired ventral and dorsal biopsies).

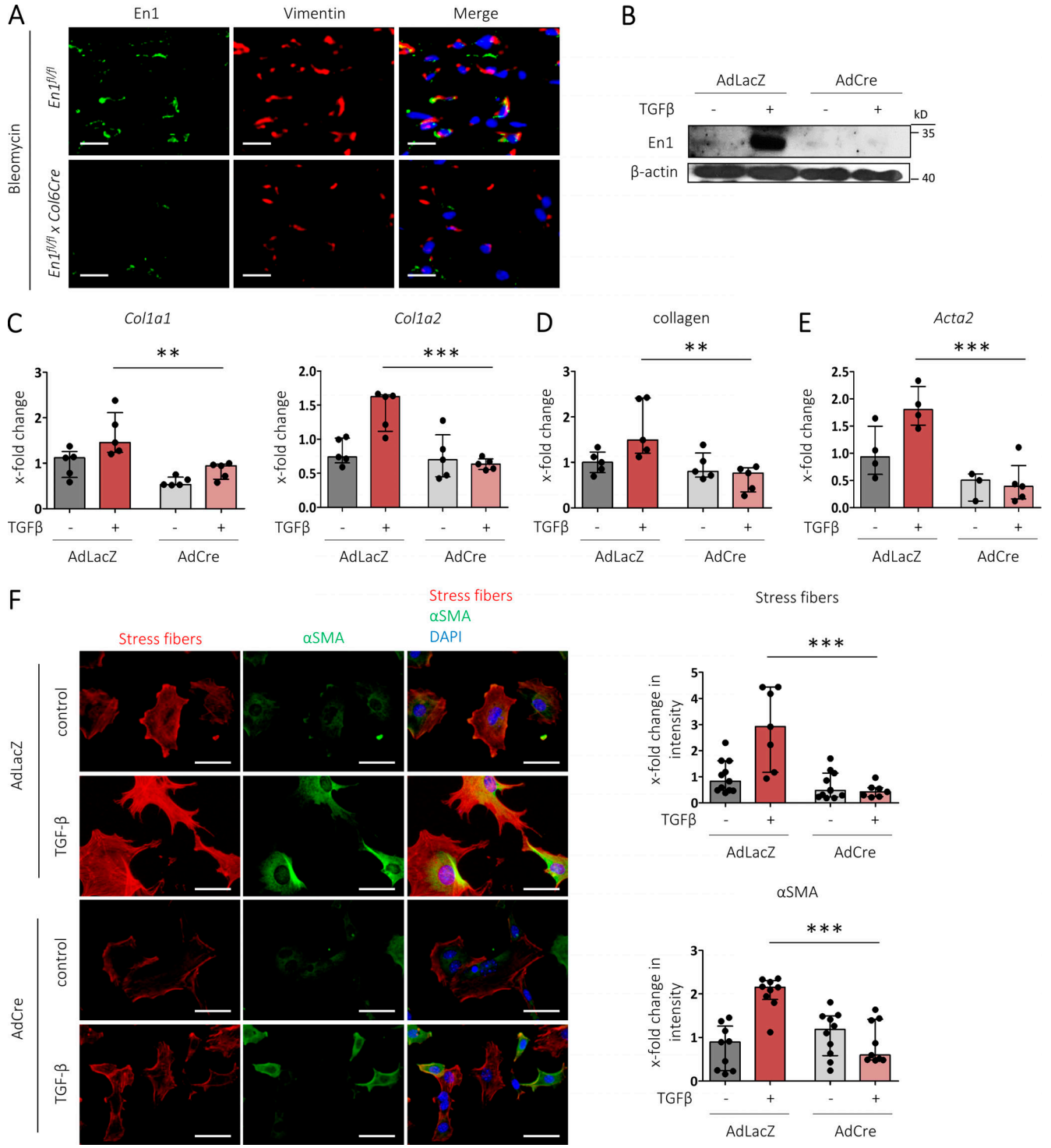

Figure S2. **Knockout of *En1* ameliorates TGFβ-induced fibroblast activation. (A)** Representative immunofluorescence stainings for En1 (green) and costaining with Vimentin (red) in the dermis of mice with fibroblast-specific knockout of *En1* and controls, both groups challenged with bleomycin, at 1,000-fold magnification (scale bars = 20 µm). Data were obtained from one experiment (n = 4). **(B)** En1 protein levels (representative Western blot images). Data were obtained from one experiment (n = 3). **(C)** Relative mRNA levels of *Col1a1* and *Col1a2*. **(D)** Secreted collagen 1 protein levels. **(E)** Relative mRNA levels of *Acta2*. Data for C–E were compiled from two independent experiments ($n \geq 4$). **(F)** Representative immunofluorescence stainings for αSMA (green) and stress fibers (red) at 400-fold magnification (scale bars = 50 µm). Quantification of signal intensity relative to control is included. Data for F were obtained from two independent experiments ($n \geq 4$). All data are represented as median ± interquartile range. P values are expressed as follows: **, 0.01 > P > 0.001; ***, P < 0.001 (ANOVA with Tukey's post hoc test).

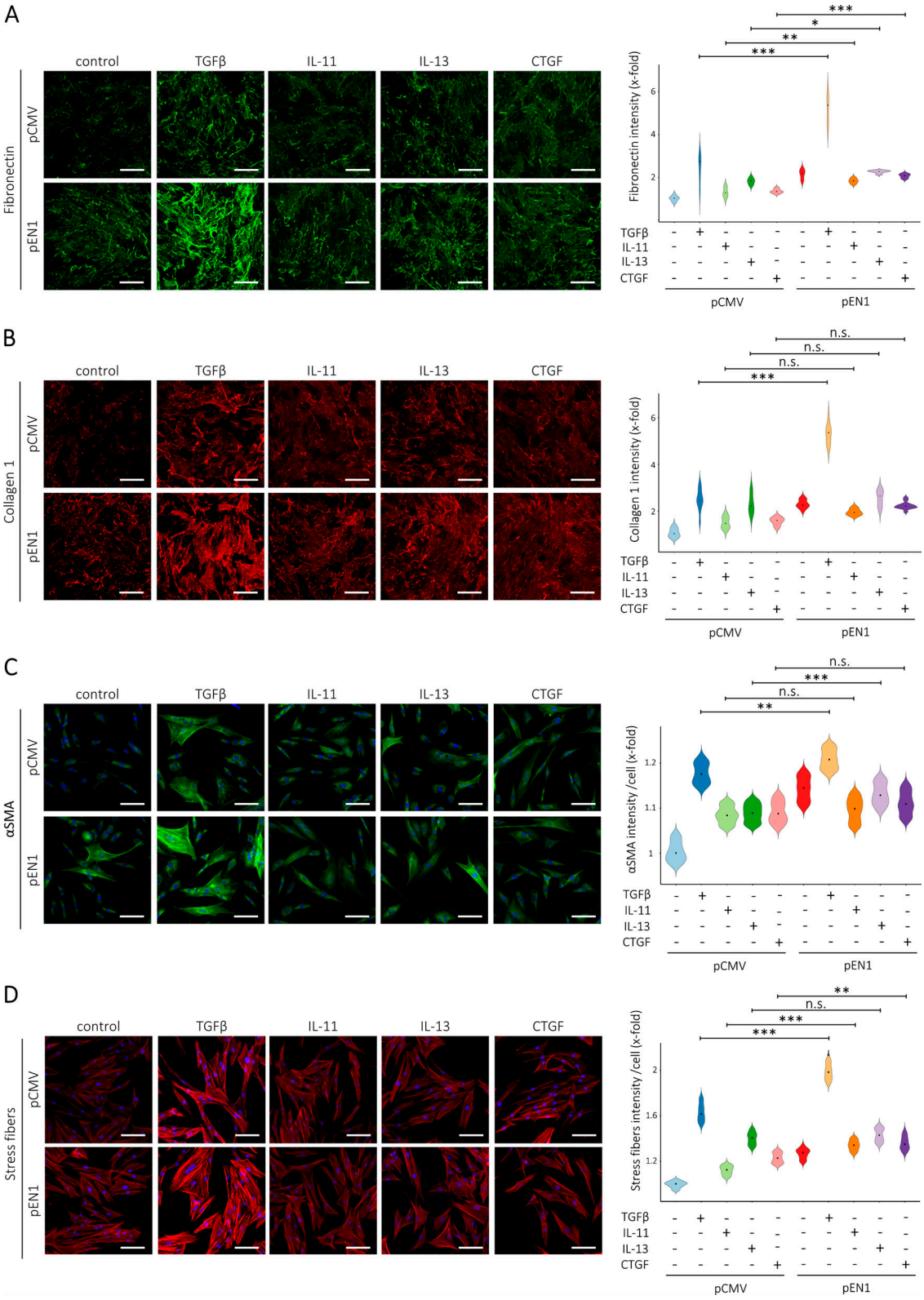

Figure S3. ***EN1* overexpression promotes IL-11–, IL-13–, and CTGF-induced fibroblast activation and ECM deposition to a lesser extent than TGFβ-induced fibroblast activation and ECM deposition. (A and B)** Representative immunofluorescence stainings for fibronectin (A) and collagen type I (B) at 100-fold magnification (scale bars = 200 µm). Quantification of average signal intensity (relative to control) is included. **(C and D)** Representative immunofluorescence stainings for αSMA (C) and stress fibers (D) at 200-fold magnification (scale bars = 100 µm). Quantification of average signal intensity for each cell line (relative to control) is included. All data are represented as median ± interquartile range of $n \geq 3$ independent biological samples per group from at least two independent experiments. P values are expressed as follows: *, 0.05 > P > 0.01; **, 0.01 > P > 0.001; ***, P < 0.001 (ANOVA with Tukey's post hoc test). Data for A–D were obtained from two independent experiments ($n = 4$).

A

TF Name	Gene Ratio (upregulated EN1-DEGs)	Gene Ratio (downregulated EN1-DEGs)	Gene Ratio (negative controls)
SP1	0.616	0.465	0.131
SP2	0.568	0.405	0.089
KLF5	0.544	0.405	0.116
ZNF263	0.532	0.356	0.087
KLF16	0.342	0.275	0.112
SP3	0.354	0.268	0.087
ZNF384	0.279	0.327	0.056
E2F6	0.369	0.246	0.129
SP8	0.309	0.218	0.084
IRF1	0.198	0.215	0.045
KLF9	0.282	0.201	0.095
MEF2C	0.186	0.180	0.074
ID4	0.183	0.176	0.058
TCF3	0.183	0.169	0.056
TCF4	0.174	0.162	0.072
FOXC2	0.156	0.158	0.021
RREB1	0.183	0.127	0.032
HOXA13	0.075	0.102	0.015
NR2C2	0.120	0.088	0.015

C2H2 zinc finger factors Fork head / winged helix factors Basic helix-loop-helix factors

B

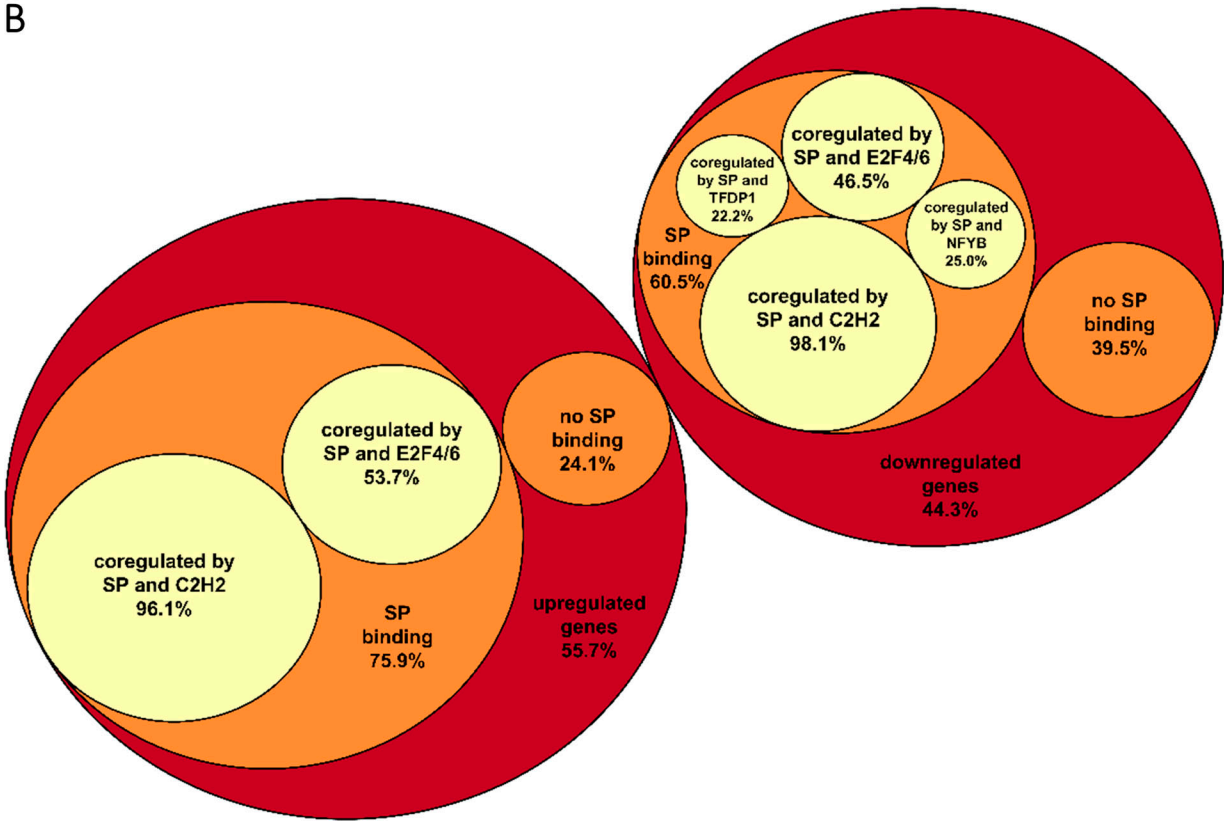

Figure S4. **EN1 promotes formation of SP1/2/3/8-containing regulatory modules with specialized profibrotic function. (A)** Transcription factors with enriched binding motifs in the promoters of up- and down-regulated EN1-DEGs, with gene ratio in EN1-DEGs (ratio of genes that contain motifs for the respective transcription factor) more than twofold higher than the gene ratio in negative controls, colored by families. **(B)** Circular packing plots illustrating predicted SP1/2/3/8 (SP) binding in the promoters of up- and down-regulated EN1-DEGs and cobinding with other members of the C2H2 or E2F families and with NFYB or TFDP1, expressed as percentages.

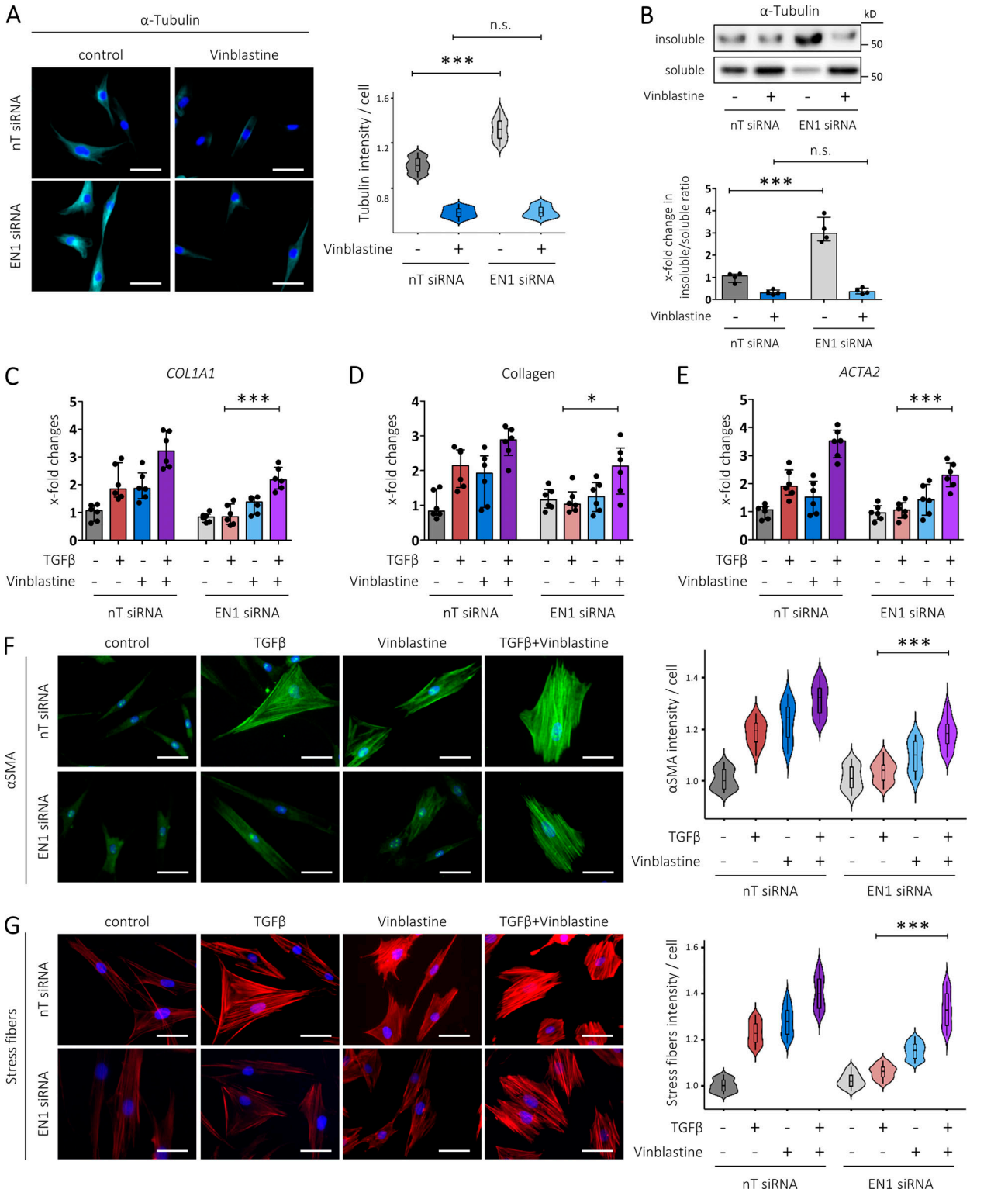

Figure S5. **Knockdown of *EN1* stabilizes the microtubular network to inhibit stress fiber formation and myofibroblast differentiation. (A and B)** Knockdown of *EN1* stabilizes microtubules. Representative immunofluorescence stainings for α-Tubulin at 400-fold magnification (scale bars = 50 µm). Quantification of total signal intensity for each cell (relative to control) is included (A). Protein levels of soluble and insoluble α-Tubulin. Representative Western blot images and quantification of insoluble/soluble α-Tubulin ratio are included (B). Data for A and B were obtained from two independent experiments ($n \geq 4$). **(C–G)** Pharmacological depolymerization of microtubules abrogates the inhibitory effects of *EN1* knockdown on TGFβ-induced myofibroblast differentiation. Relative mRNA levels of *COL1A1* (C). Relative protein levels of secreted collagen type I (D). Relative mRNA levels of *ACTA2* (E). Representative immunofluorescence stainings for αSMA (F) and stress fibers (G) at 400-fold magnification (scale bars = 50 µm). Data for C–G were obtained from two independent experiments ($n \geq 4$). Quantification of average signal intensity for each cell (relative to control) is included. All data are represented as median ± interquartile range. P values are expressed as follows: *, 0.05 > P > 0.01; **, 0.01 > P > 0.001; ***, P < 0.001 (ANOVA with Tukey's post hoc test).

Provided online are six tables. Table S1 lists primers used for quantitative real-time PCR. Table S2 shows the clinical data of SSc patients. Table S3 lists the antibodies used in the imaging CyToF panel. Table S4 shows transcription factor binding site enrichments in the promoters of EN1-DEGs. Table S5 shows transcription factor binding site enrichments in the promoters of EN1-SP-DEGs. Table S6 shows functional enrichment analysis of EN1-SP-DEGs.